© 2013. Published by The Company of Biologists Ltd | Development (2013) 140, 4691-4702 doi:10.1242/dev.098616

RESEARCH ARTICLE

STEM CELLS AND REGENERATION

Genome-wide analysis of the bHLH gene family in planarians identifies factors required for adult neurogenesis and neuronal regeneration

Martis W. Cowles[1], David D. R. Brown[2,3], Sean V. Nisperos[1], Brianna N. Stanley[1], Bret J. Pearson[2,3,4] and Ricardo M. Zayas[1,*]

ABSTRACT

In contrast to most well-studied model organisms, planarians have a remarkable ability to completely regenerate a functional nervous system from a pluripotent stem cell population. Thus, planarians provide a powerful model to identify genes required for adult neurogenesis *in vivo*. We analyzed the basic helix-loop-helix (bHLH) family of transcription factors, many of which are crucial for nervous system development and have been implicated in human diseases. However, their potential roles in adult neurogenesis or central nervous system (CNS) function are not well understood. We identified 44 planarian bHLH homologs, determined their patterns of expression in the animal and assessed their functions using RNAi. We found nine bHLHs expressed in stem cells and neurons that are required for CNS regeneration. Our analyses revealed that homologs of *coe*, *hes* (*hesl-3*) and *sim* label progenitors in intact planarians, and following amputation we observed an enrichment of *coe*$^+$ and *sim*$^+$ progenitors near the wound site. RNAi knockdown of *coe*, *hesl-3* or *sim* led to defects in CNS regeneration, including failure of the cephalic ganglia to properly pattern and a loss of expression of distinct neuronal subtype markers. Together, these data indicate that *coe*, *hesl-3* and *sim* label neural progenitor cells, which serve to generate new neurons in uninjured or regenerating animals. Our study demonstrates that this model will be useful to investigate how stem cells interpret and respond to genetic and environmental cues in the CNS and to examine the role of bHLH transcription factors in adult tissue regeneration.

KEY WORDS: Basic helix-loop-helix, *Coe*, *Single-minded*, *Hes*, Neurogenesis, Lophotrochozoan, Planarians, Regeneration, *Schmidtea mediterranea*, Stem cells, Neoblasts

INTRODUCTION

The discovery that neurogenesis persists in the central nervous system (CNS) of adult animals (Gage, 2002) changed a long-held doctrine that neurons were only produced in the embryo (Ramón y Cajal, 1928; Kempermann, 2011). Although it is now well accepted that adult neurogenesis is a widespread phenomenon across diverse metazoans (Lindsey and Tropepe, 2006; Kempermann, 2012), the ability of most organisms to produce new neurons does not compensate for cells lost after injury or disease. Therefore, to examine how neural precursors could be directed to repair CNS neurons *in vivo*, comparative approaches using animal models of regeneration will help us to gain insights into the basic mechanisms needed to reestablish nervous system function after injury or the onset of neurodegenerative disease (Kempermann, 2011).

Freshwater planarians have emerged as an excellent model to examine the molecular mechanisms underlying stem cell biology and tissue replacement (Elliott and Sánchez Alvarado, 2013; King and Newmark, 2012). Following amputation, planarians are capable of restoring lost body parts from a population of adult pluripotent stem cells called neoblasts (Baguñà, 2012; Elliott and Sánchez Alvarado, 2013). Planarian stem cells share conserved pluripotency determinants with mammalian stem cells (Labbé et al., 2012; Önal et al., 2012; Solana et al., 2012) and serve to replace cells lost during normal physiological cell turnover or after amputation. In contrast to most model organisms currently studied, planarians have the remarkable ability to regenerate their CNS after injury. Thus, these animals provide an excellent opportunity to analyze mechanisms underlying stem cell regulation and CNS regeneration *in vivo*. The planarian CNS consists of bi-lobed cephalic ganglia (brain) that are connected to two longitudinal ventral nerve cords projecting posteriorly along the length of the animal. Distinct neuronal cell types have been described by histochemistry, including unipolar and bipolar neurons as well as neurosecretory cells (Bullock and Horridge, 1965; Lentz, 1968). The generation of genomic resources has led to identification of hundreds of neural markers that have been used to show that the planarian CNS is molecularly complex (Gentile et al., 2011), but little is known about how these animals regenerate their nervous system. On the basis of elegant single cell transplantation studies in lethally irradiated planarians (Wagner et al., 2011), it has been estimated that less than 5% of the planarian stem cells are truly pluripotent (Rink, 2013). Therefore, we and others hypothesize that a fraction of the heterogeneous stem cell pool may be comprised of lineage-committed or specialized progenitor cells (Reddien, 2013). To fully understand the mechanisms underlying how neuronal diversity is maintained or reestablished in planarians it will be essential to define any neural precursor populations that may exist.

Transcription factors from the basic helix-loop-helix (bHLH) gene family play vital regulatory roles throughout the different stages of neurogenesis in embryos, including neural fate commitment, subtype specification, migration and axon guidance (Bertrand et al., 2002; Guillemot, 2007). Genes of the *Drosophila achaete-scute* complex represent the prototypical proneural genes that are important for development of the peripheral and central nervous systems (Jan and Jan, 1994). Proneural genes have been identified

[1]Department of Biology, San Diego State University, San Diego, CA 92182, USA. [2]The Hospital for Sick Children, Program in Developmental and Stem Cell Biology, Toronto, ON M5G 0A4, Canada. [3]University of Toronto, Department of Molecular Genetics, Toronto, ON M5S 1A8, Canada. [4]Ontario Institute for Cancer Research, Toronto, ON M5G 1L7, Canada.

*Author for correspondence (rzayas@mail.sdsu.edu)

Received 4 May 2013; Accepted 12 September 2013

Development (2013) doi:10.1242/dev.098616

in sponges (Richards et al., 2008) and their roles are conserved from cnidarians to vertebrates (Lindsey and Tropepe, 2006; Galliot et al., 2009). However, the precise function of bHLH genes in embryos or adult neural stem cells remains poorly understood (Kintner, 2002). Here we have performed a genome-wide analysis of bHLH family genes to identify factors essential for CNS tissue renewal in adult planarians. Our screen identified nine genes that are expressed in both the stem cells and neurons and are required for normal CNS regeneration, including homologs of *collier/olfactory-1/early B-cell factor* (*coe*), *hairy/enhancer of split* (*hes-like-3*) and *single-minded* (*sim*). To characterize and follow the fate of coe^+, $hesl\text{-}3^+$ and sim^+ stem cells, we performed bromodeoxyuridine (BrdU) pulse-chase experiments and found that *coe* and *sim* are expressed in proliferating cells adjacent to the CNS, which can be traced to the brain or ventral nerve cords over the course of 2 days. During regeneration, we observed an enrichment of coe^+ and sim^+ progenitors near the wound site. Furthermore, RNAi knockdown of *coe*, *hesl-3* or *sim* led to defects in CNS regeneration, including failure of the cephalic ganglia to reconnect or pattern, and a loss of expression of genes unique to distinct neuronal subtypes. Together, these data suggest that *coe*, *hesl-3* and *sim* are expressed in neural progenitor cells and that these bHLH genes are required to generate new neurons in uninjured and regenerating animals. Our study demonstrates that this model will be useful to investigate how stem cells interpret and respond to genetic and environmental cues in the CNS and to examine the role of bHLH transcription factors in adult tissue regeneration.

RESULTS

Identification of bHLH family genes in planarians

We identified 44 sequences in the planarian *Schmidtea mediterranea* predicted to encode a bHLH motif and named them according to their homology, as described in the Materials and methods (supplementary material Fig. S1, Table S1; for brevity we have omitted the *Smed* prefix from the gene names). Recent transcriptional profiles generated from sorted cell populations indicate that most bHLH homologs are expressed in the planarian stem cells and their postmitotic progeny (Labbé et al., 2012; Önal et al., 2012; Resch et al., 2012). To investigate cell- and tissue-specific patterns of bHLH gene expression, we performed whole mount *in situ* hybridization (WISH). We confirmed the presence of transcripts in stem cell or their progeny by testing for the loss of gene expression throughout the parenchyma (mesenchyme) 6 days following exposure to γ-irradiation, a treatment that depletes all stem cells and postmitotic progeny (Reddien et al., 2005b; Eisenhoffer et al., 2008). Consistent with the transcriptome data, we found that 35/43 bHLH genes tested are expressed in stem cells and their progeny (supplementary material Table S1). As expected, we also observed bHLH expression in differentiated tissues, including the CNS (21 genes), epidermis (three genes), pharynx (14 genes) or intestine (nine genes) (supplementary material Fig. S2, Table S1). One gene, *neuroD-2*, was not detected by WISH.

A subset of bHLH genes is expressed in neurons

Of the 12 CNS- and stem-cell-expressed bHLH genes, we selected *atoh*, *coe*, *fer3l-1*, *hesl-3* and *sim* for detailed expression analyses because their transcripts were detected in discrete cell populations (supplementary material Fig. S2). To confirm the pattern of mRNA expression in the CNS and visualize the distribution of these cell populations in reference to the brain, we performed double-fluorescent *in situ* hybridization experiments (dFISH) using the pan-neural marker *pc2* (Collins et al., 2010). *atoh*, *coe*, *fer3l-1*, *hesl-3* and *sim* were expressed in discrete neural populations throughout the brain and in regenerating tissues (Fig. 1; supplementary material Fig. S3). In addition, *fer3l-1* (supplementary material Fig. S3D), *hesl-3* (Fig. 1D) and *sim* (Fig. 1G) were detected in cells distributed throughout the mesenchyme. We then investigated the expression of *coe*, *hesl-3* and *sim* in specific neuronal subtypes by performing dFISH with markers of cholinergic, GABAergic, octopaminergic, dopaminergic and serotonergic neurons (Umesono et al., 2011). *coe*, *hesl-3* and *sim* were each co-expressed in cholinergic neurons (Fig. 1J-L). We also detected transcripts for *coe* in GABAergic, octopaminergic, dopaminergic and serotonergic neurons and *sim* in octopaminergic and dopaminergic neurons (Fig. 1J,L). These results demonstrate that a subset of bHLH genes is expressed in molecularly distinct differentiated neurons.

coe, *hesl-3* and *sim* label cycling cells in close proximity to the CNS

Following amputation, stem cells proliferate beneath the wound site (post-blastema) and give rise to the regeneration blastema, the structure where postmitotic cells differentiate to form the missing tissues. *atoh*, *coe*, *fer3l-1*, *hesl-3* and *sim* were expressed in the newly regenerated tissues, but it was also noted that these mRNAs were present in cells located in the post-blastema (Fig. 1; supplementary material Fig. S3). Therefore, we examined whether *atoh*, *coe*, *fer3l-1*, *hesl-3* and *sim* could be detected in mitotic cells. We found that, with the exception of *atoh*, their transcripts could be visualized in a subset of anti-phosphohistone-$H3^+$ cells (Fig. 1C,F,I; supplementary material Fig. S3C,F), which we also observed in uninjured planarians (data not shown).

To distinguish between gene expression in stem cells/progeny or differentiated neurons, we examined the expression of *atoh*, *coe*, *fer3l-1*, *hesl-3* and *sim* following 6 days of γ-irradiation treatment. Compared with control animals, *atoh* expression was reduced throughout the mesenchyme, but we were unable to detect changes in expression in the head or the pre-pharyngeal area even when we used FISH (supplementary material Fig. S3G-J′). In contrast to *atoh*, we observed a reduction of coe^+ cells near the brain and between the cephalic ganglia and ventral nerve cords (VNCs) (supplementary material Fig. S3K,K′). *fer3l-1* expression was broadly reduced in the mesenchyme, except for a few cells located on the dorsal surface of the cephalic ganglia and distributed throughout the mesenchyme (supplementary material Fig. S3L,L′). *hesl-3* and *sim* staining were also reduced in the mesenchyme and near the cephalic ganglia following γ-irradiation (supplementary material Fig. S3M-N′). To validate further that *coe*, *hesl-3* and *sim* were expressed in a subset of stem cells, we co-stained these genes with the stem cell marker *smedwi-1* (Reddien et al., 2005b; Eisenhoffer et al., 2008) (Fig. 1M-O). Taken together, our analyses confirmed that bHLH genes were expressed in subsets of stem cells and postmitotic progeny. In addition, we noted that cell populations that expressed *coe*, *hesl-3* and *sim* near the CNS were γ-irradiation-sensitive, further supporting potential roles of these genes in differentiation of neural precursor-like cells.

coe and *sim* are expressed in differentiating neurons

Stemming from our observations that *coe*, *hesl-3* and *sim* were expressed in stem cells and in diverse neural subtypes, we reasoned that these genes label lineage-committed progenitors and differentiating neurons. To address this possibility, we sought to label stem cells expressing *coe*, *hesl-3* or *sim* and map their relative positions in the animal over time. Although the most commonly used tools to trace cell lineages (e.g. genetic marks) (Kretzschmar

Development (2013) doi:10.1242/dev.098616

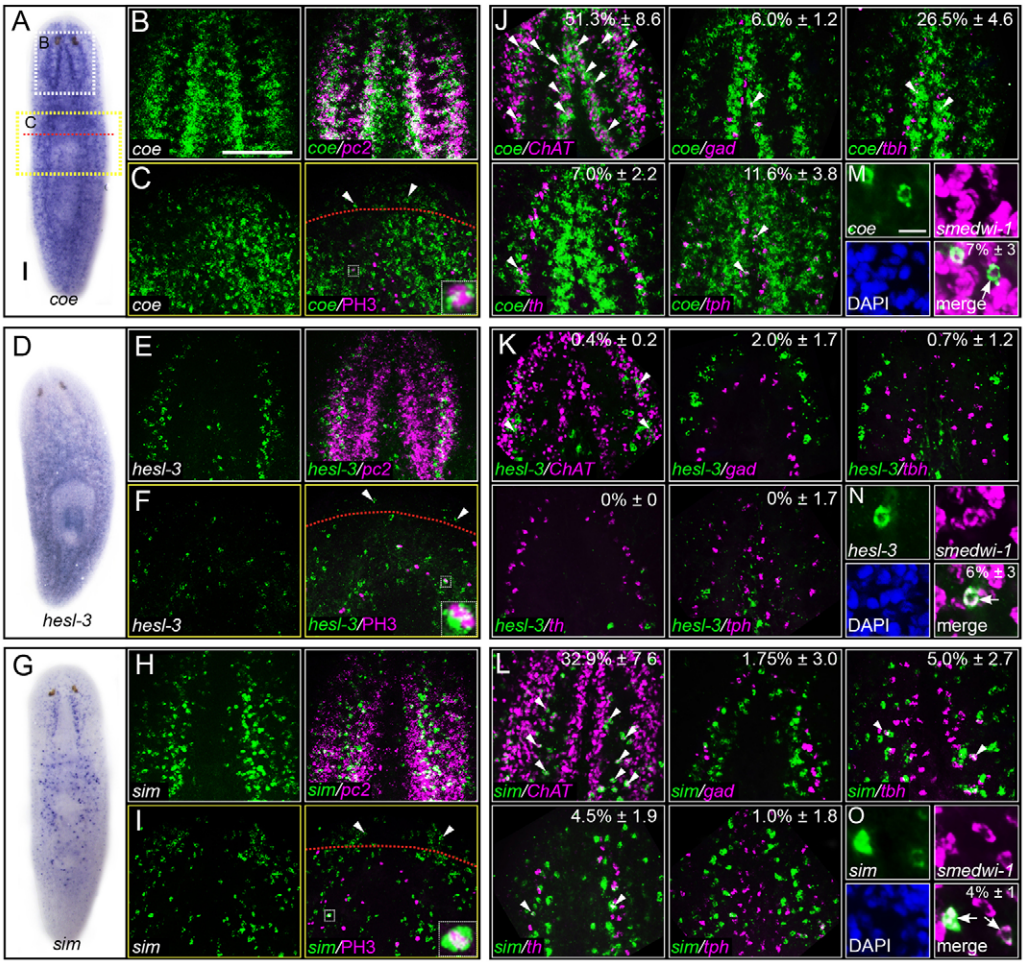

Fig. 1. *coe*, *hesl-3* and *sim* are expressed in stem cells and neurons. (A) Expression pattern of *coe*. Dashed boxes indicate zoom area of the brain or regeneration blastema shown in B and C, respectively. Dashed red line indicates site of amputation. (B) FISH to *coe* (green) and *pc2* (magenta). (C) Animals processed for FISH to *coe* and counterstained with anti-phosphohistone-H3 (ph3) to label mitotic cells in 3-day regenerates. Arrowheads denote *coe*$^+$ cells within the blastema. D-F and G-I show similar analyses for *hesl-3* and *sim*, respectively. White dashed boxes in C, F and I highlight *bHLH*/ph3-positive cells shown at high magnification within merged image insets. (J-L) Animals were processed for dFISH to *coe*, *hes-3* or *sim* and markers of cholinergic (*ChAT*, *choline acetyltransferase*), GABAergic (*gad*, *glutamic acid decarboxylase*), octopaminergic (*tbh*, *tyramine β-hydroxylase*), dopaminergic (*th*, *tyrosine hydroxylase*) and serotonergic (*tph*, *tryptophan hydroxylase*) neurons. White arrowheads point to co-labeled cells. (M-O) Representative photos of cells imaged at high magnification from animals that were processed for dFISH to *coe*, *hesl-3* or *sim* and *smedwi-1* and counterstained with DAPI. The percentage of the total number of subtype-specific neurons or *smedwi-1*$^+$ cells that co-expressed *coe*, *hesl-3* or *sim* are shown in J-O. Scale bars: 100 μm in A,B; 10 μm in M.

and Watt, 2012) are not yet available in planarians, it is possible to label S-phase neoblasts with the thymidine analog BrdU and then determine the location of label-retaining cells (Newmark and Sánchez Alvarado, 2000; Eisenhoffer et al., 2008). This approach has been used to study planarian eye (Lapan and Reddien, 2011) and intestinal (Forsthoefel et al., 2011) cell differentiation. Previous studies have estimated that the length of S/G2/M in planarians is between 12 and 16 hours (Newmark and Sánchez Alvarado, 2000). We predicted that at later time points BrdU$^+$ cells in the head marked by any of these bHLH genes would represent differentiating stem cells. Accordingly, we noted that, as expected, *coe*$^+$ and *sim*$^+$ cells were *smedwi-1*$^-$ in the anterior region of the brain (supplementary material Fig. S4). We pulsed animals with BrdU and inspected animals for BrdU$^+$ and *coe*$^+$, *hesl-3*$^+$ or *sim*$^+$ cells in the head, pre-pharyngeal and post-pharyngeal areas after a 4-, 24- or 48-hour chase period (Fig. 2). We found that most double-labeled cells were located in the head and pre-pharyngeal regions, and we focused our analyses on these areas.

Following a 4-hour chase, BrdU$^+$/*coe*$^+$ cells were located throughout the mesenchyme of the head, pre- and post-pharyngeal regions, with some cells in close proximity to the brain and VNCs (Fig. 2A,A′). Over time, BrdU$^+$/*coe*$^+$ progeny were detected in more anterior and lateral regions of the cephalic ganglia or directly adjacent to the VNCs (Fig. 2B,C). After 4 hours, BrdU$^+$/*sim*$^+$ cells were only detected in the pre- and post-pharyngeal areas (Fig. 2D,D′). Similar to *coe*$^+$ progenitors, BrdU$^+$/*sim*$^+$ cell populations could be traced to the CNS over time; by 24 hours, progenitors were observed near the posterior end of the brain, and by 48 hours, we observed BrdU$^+$/*sim*$^+$ cells at the most anterior tip of the cephalic ganglia (Fig. 2E,F). Cells progressing through S-phase that expressed *hesl-3* were observed throughout the animal (Fig. 2G,G′). In contrast to *coe*$^+$ and *sim*$^+$ progenitors, the distribution of BrdU$^+$/*hesl-3*$^+$ cells remained relatively consistent over the course of 48 hours (Fig. 2H,I). To determine whether *coe*, *hesl-3* and *sim* label unique cell populations, we performed dFISH to either *coe* or *hesl-3* with *sim*. We found that *coe*, *hesl-3* and *sim* were not co-expressed in the head; however, although rare, we did observe *coe*$^+$/*sim*$^+$ cells in the pre-pharyngeal area (supplementary material Fig. S5A-E). Consistent with the expression of these genes in *smedwi-1*$^+$ cells, these data suggest that *coe*, *hesl-3* and *sim* are expressed in lineage-committed progenitors. Moreover, we observed *coe*$^+$ and *sim*$^+$ progenitors near the CNS over time, suggesting that these genes are expressed in differentiating neurons.

In addition to determining the location of BrdU$^+$ cells marked by bHLHs, we quantified the number of double-positive cells over time (Fig. 2J-M). After 4 hours, BrdU$^+$/*coe*$^+$ cells comprised ~3.7% of BrdU$^+$ cells in the head or pre-pharyngeal area (Fig. 2K). Interestingly, by 48 hours, we observed an increase in the proportion of BrdU$^+$/*coe*$^+$ in both the head (9.5%) and pre-pharyngeal region (10%; Fig. 2K). Similar to *coe*$^+$ progenitors, the proportion of BrdU$^+$/*sim*$^+$ cells also increased over time (Fig. 2L). By contrast, the proportion of BrdU$^+$/*hesl-3*$^+$ cells remained consistent throughout the head and pre-pharyngeal area over the course of 48 hours (Fig. 2M). Intriguingly, we also noted that after 48 hours we still observed

Development (2013) doi:10.1242/dev.098616

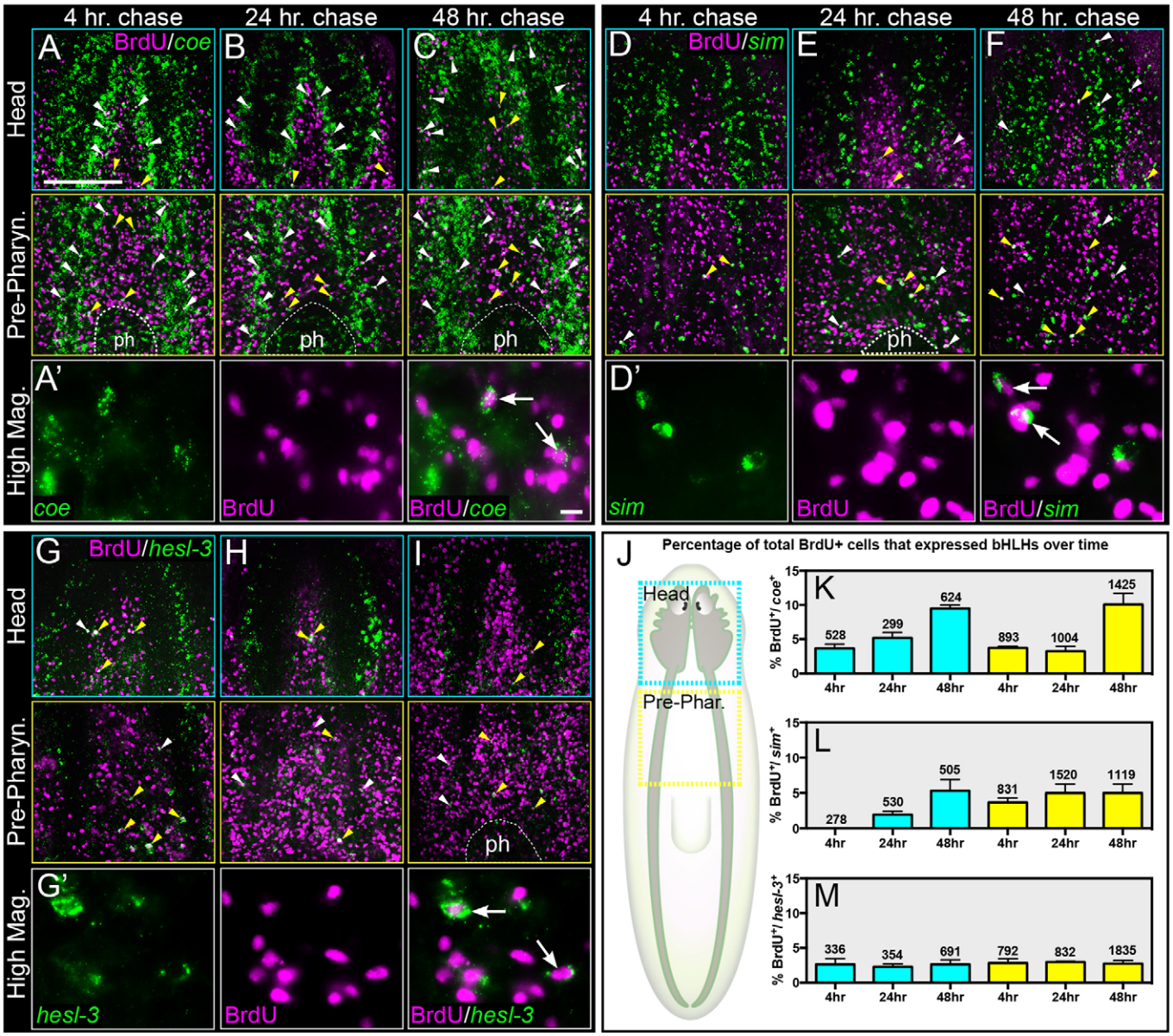

Fig. 2. Birthdating of *coe*$^+$, *hesl-3*$^+$ and *sim*$^+$ progenitors. (A-C) Intact animals were pulsed with BrdU, followed by a 4-, 24- or 48-hour chase and stained for BrdU and *coe*. Arrowheads point to BrdU$^+$/*coe*$^+$ cells near the CNS (white) or the mesenchyme (yellow). (A′) High magnification of animals in A; the arrows indicate BrdU$^+$/*coe*$^+$ cells. Similar analyses for *sim* and *hesl-3* are shown in D-F and G-I, respectively. (J) Cartoon depicting the regions counted in K-M. (K-M) Percentage of the total number of BrdU$^+$ cells that are *coe*$^+$, *hesl-3*$^+$ or *sim*$^+$ following a 4, 24- or 48-hour pulse; numbers correspond to the total number of BrdU$^+$ cells counted. Blue and yellow bars indicate cell counts from the head and pre-pharyngeal regions, respectively. Scale bars: 100 μm in A; 10 μm in A′. ph, pharynx.

BrdU$^+$ cells expressing *coe*, *hesl-3* or *sim* in the pre-pharyngeal area (yellow arrowheads in Fig. 2C,F,I), the same location where most *coe*$^+$, *hesl-3*$^+$ and *sim*$^+$ cycling cells were first detected following a 4-hour chase period (Fig. 2A,D,G), which suggests that new progenitors were generated or differentiating cells turned on expression of these genes. The increase in the proportion of BrdU$^+$ cells that expressed *coe* or *sim* near the brain and VNCs, combined with the observation that these genes were expressed in diverse neuronal subtypes (Fig. 1J,L), demonstrate that at least some *coe*$^+$ and *sim*$^+$ progenitors differentiate into neurons. The fact that we did not observe changes in the proportion of *hesl-3* suggests a potential role of this gene in progenitor cell maintenance (Ishibashi et al., 1995; Kageyama et al., 2008).

In addition, we investigated whether these *coe*$^+$ and *sim*$^+$ progenitor populations contribute to the generation of the regeneration blastema following amputation. By 2 and 3 days of regeneration, BrdU$^+$/*coe*$^+$ and BrdU$^+$/*sim*$^+$ cells were detected in the post-blastema of animals regenerating new heads, with most BrdU$^+$/*coe*$^+$ progenitors located directly adjacent to the VNCs and many BrdU$^+$/*sim*$^+$ progenitors located between the VNCs (Fig. 3A-D). In *S. mediterranea*, head regeneration is completed within 7 days following amputation, and we found that the distribution of BrdU$^+$/*coe*$^+$ or BrdU$^+$/*sim*$^+$ cells observed in uninjured animals was reestablished by this time point (Fig. 2A,D, Fig. 3G-J). Taken together, these data are consistent with the hypothesis that the blastema is generated from a heterogeneous population of lineage-committed cells (Reddien, 2013).

Development (2013) doi:10.1242/dev.098616

FGF signaling modulates expression of *sim*$^+$ and *coe*$^+$ neurons and progenitors

Gene silencing of *nou-darake* (*ndk*), an FGF receptor-like gene, disrupts anterior patterning and leads to ectopic expression of brain-specific neurons outside of the head domain (Cebrià et al., 2002). We hypothesized that *ndk* silencing would cause an increase in the number of *coe*$^+$ and *sim*$^+$ progenitor cells. As we expected, ectopic expression of brain-specific markers (*npp-4* and *gpas*) extended from the posterior end of the brain to the anterior boundary of the pharynx following 14 days of *ndk* RNAi treatment (Fig. 4A,B). We then examined *sim* and *coe* mRNA expression in the pre-pharyngeal area of control and *ndk*(*RNAi*) animals after 14 days of RNAi; we also exposed animals from each RNAi group to a lethal dose of γ-irradiation to distinguish stem cell or progeny expression from differentiated neurons (Fig. 4C-E). In control animals, we consistently observed *coe*$^+$ and *sim*$^+$ cells in the pre-pharyngeal region and found that most irradiation-sensitive cells were located between the VNCs. Following *ndk* RNAi, we found there were nearly twice the number of *coe*$^+$ and ~40% more *sim*$^+$ cells between the VNCs (Fig. 4F-H). Irradiated *ndk*(*RNAi*) animals confirmed that the majority of the additional cells between the VNCs are stem cells or early progeny. We conclude that *coe*$^+$ and *sim*$^+$ progenitor generation is regulated by signals downstream of FGF signaling.

Analysis of bHLH gene function in CNS regeneration

We took advantage of the experimental ease to inhibit gene function in planarians by RNAi to investigate the role of all 44 bHLH genes in planarian tissue regeneration. To screen for defects in CNS architecture and stem cell regulation, animals were stained with the pan-neural marker anti-SYNAPSIN and the mitotic cell marker anti-phosphohistone-H3 following dsRNA treatment (supplementary material Fig. S6A). We observed a wide range of regeneration phenotypes following RNAi knockdown of 11 bHLH genes, including lesions (*mitfl-1*), defects in CNS morphology (*arnt*, *arh*, *atoh8-1*, *coe*, *da*, *max*, *mxi-1* and *sim*) and patterning (*hesl-3* and *myoD*) (Table 1; supplementary material Fig. S6B). We did not observe obvious defects in cell division following knockdown of any bHLH gene (data not shown). *mitfl-1* was primarily detected in differentiated intestinal cells (supplementary material Fig. S2), and gene knockdown caused severe regeneration abnormalities and dorsal lesions that resulted in death, a phenotype reminiscent of defects observed after the loss of intestinal integrity (Forsthoefel et al., 2012). Consistent with previous reports, gene silencing of *tfc15* (Wagner et al., 2011) resulted in no discernible phenotype, whereas *myoD* RNAi caused regeneration blastema patterning defects (Reddien et al., 2005a).

Proneural bHLHs form heterodimers with ubiquitously expressed E proteins (such as *daughterless*, *da*) to bind DNA and function to commit progenitors to the neural fate during development (Bertrand et al., 2002). We did not observe regeneration defects following RNAi of candidate proneural gene homologs, such as *acheate-scute* or *neuroD*, which we validated by real-time quantitative PCR and found that our treatment strongly silenced each gene that we tested (supplementary material Fig. S6C). It has been shown that developmental defects are exacerbated in *Drosophila* when proneural factors are co-silenced with *da* (Goulding et al., 2000; Huang et al., 2000). Therefore, we performed double-RNAi experiments of *da* and *ascl-1*, *ascl-2*, *atoh*, *neuroD-1* or *neuroD-2*. We also co-silenced predicted bHLH paralogs to test if genes may be functionally redundant (*ascl-1;ascl-2* and *hesl-1;hesl-2* RNAi). Due to the possibility that these proteins perdure, we also conducted long-term knockdown experiments (6 weeks of RNAi treatment; *ascl-1*, *ascl-2*, *hesl-1*, *hesl-2*, *sim*). Neither combinatorial nor long-term RNAi experiments revealed any additional regeneration defects. However, extended knockdown experiments increased the penetrance of *sim*(*RNAi*) animals from ~50% to 100% (*n*=10/10; data not shown).

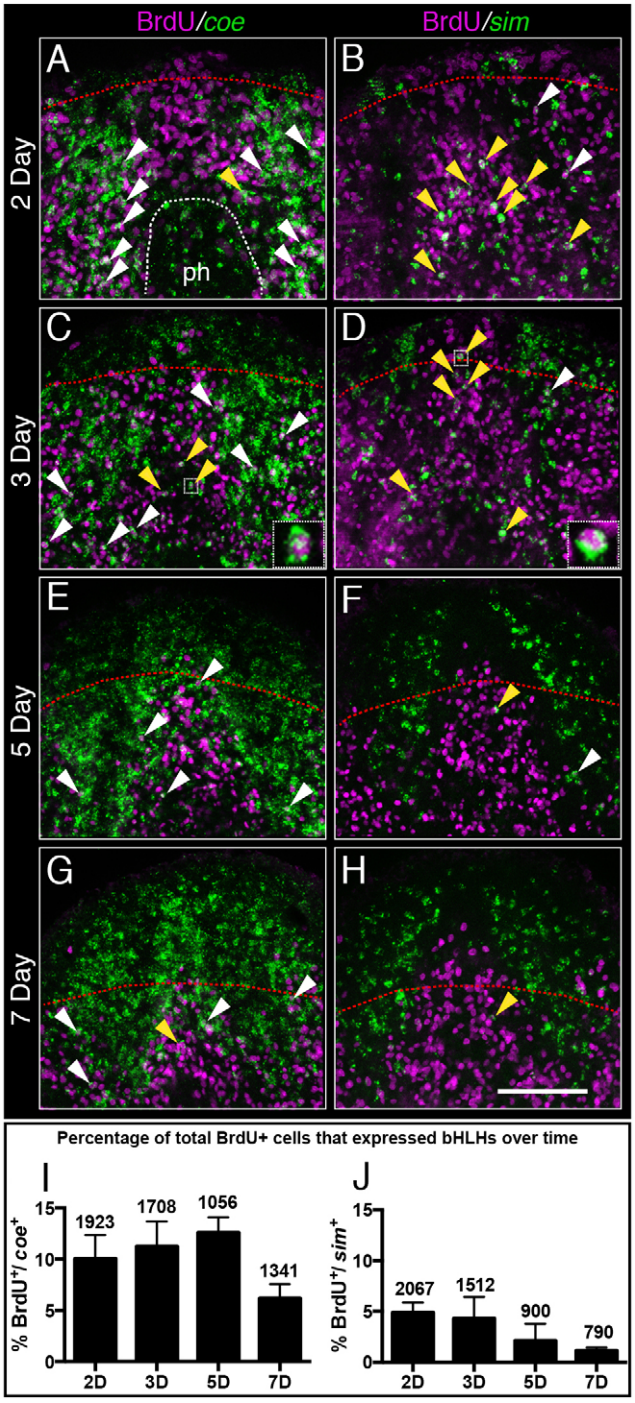

Fig. 3. Analysis of *coe*$^+$ and *sim*$^+$ cycling cells during regeneration. (A-H) 2, 3, 5 and 7 day regenerates were soaked in BrdU for 1 hour, chased for 4 hours, and co-labeled for *coe* or *sim* and BrdU. Red line denotes amputation site. Yellow and white and arrowheads indicate *coe*$^+$/BrdU$^+$ or *sim*$^+$/BrdU$^+$ cells that are in the mesenchyme or in close proximity to the CNS, respectively. (I,J) Percentages of total BrdU$^+$ cells that were *coe*$^+$ or *sim*$^+$ at each time point. Numbers above each bar correspond to the total number of BrdU$^+$ cells counted. ph, pharynx. Scale bar: 100 μm.

Development (2013) doi:10.1242/dev.098616

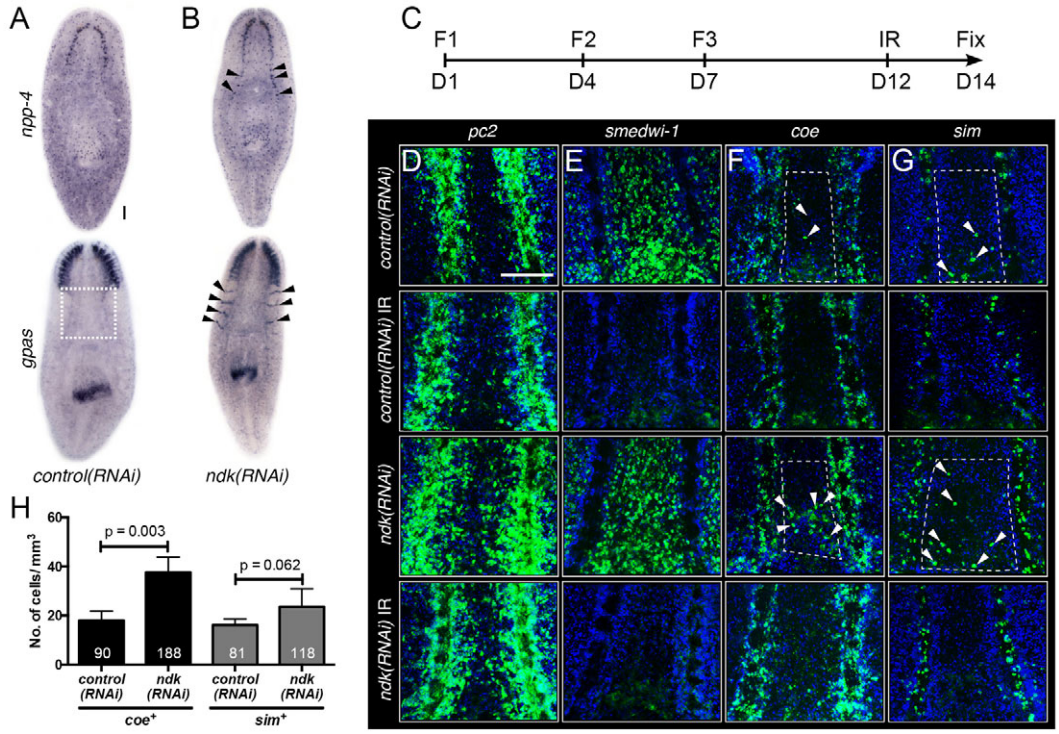

Fig. 4. Induction of ectopic neurogenesis causes an increase in the number of *coe*$^+$ and *sim*$^+$ neurons and progenitors. (A,B) *control*(*RNAi*) and *ndk*(*RNAi*) animals were processed for WISH to *npp-4* and *gpas* (*n*=10). Arrows point to ectopic *npp-4*$^+$ or *gpas*$^+$ cells. White dashed box shows region imaged in D-G. (C) Schematic showing RNAi feeding (F, feeding; D, days) and γ-irradiation (IR) schedule for animals shown in D-G. (D-G) RNAi animals were processed for FISH to *pc2*, *smedwi-1*, *coe* or *sim* and counterstained with DAPI (blue) (*n*=15). (H) Quantification of *coe*$^+$ and *sim*$^+$ progenitors within white boxed areas in F-G; total number of cells counted are indicated within each bar. Scale bars: 100 μm.

Furthermore, we capitalized on the robust *ndk* RNAi phenotype to test the hypothesis that bHLHs required for neurogenesis would suppress ectopic nervous system expansion. We performed combinatorial RNAi experiments using *ndk*, which has been successfully used to investigate the role of other genes in planarian body patterning and CNS regeneration (Felix and Aboobaker, 2010; Iglesias et al., 2011; Blassberg et al., 2013), and screened 15 genes (*ascl-1*, *ascl-2*, *atoh*, *atoh8-1*, *coe*, *da*, *hesl-1*, *-2*, *-3*, *hlh*, *id4*, *neuroD-1*, *neuroD-2*, *sim* and *usf*) by inspecting *bHLH;ndk*(*RNAi*) animals for changes in *gpas* and *npp-4* expression. Induction of *gpas* expression posterior to the cephalic ganglia was not suppressed by inhibiting any of the bHLH genes together with *ndk*. However, *ascl-1;ndk*(*RNAi*) animals exhibited a 60% decrease in ectopic *npp-4*$^+$ cells, whereas *ndk;hesl-3*(*RNAi*) and *ndk;neuroD-1*(*RNAi*) animals exhibited a 40% decrease of ectopic *npp-4*$^+$ cells when compared with *gfp;ndk*(*RNAi*) animals (supplementary material Fig. S7A-G). These data suggest that *ascl-1* and *neuroD-1* may function in neural specification, but do not cause gross morphological CNS regeneration defects following gene knockdown.

coe, *hesl-3* and *sim* are required for neuronal regeneration or maintenance

Our RNAi screen revealed that *coe*, *hesl-3* or *sim* led to clear defects in brain regeneration (Fig. 5A-D). *coe*(*RNAi*) regenerates displayed photoreceptors with abnormal morphology and smaller cephalic ganglia that failed to form anterior commissures (*n*=94/114; Fig. 5B). In *hesl-3*(*RNAi*) regenerates, the CNS was abnormally patterned, with animals regenerating a single or an ectopic eyespot and brains with abnormal morphology (*n*=20/35; Fig. 5C). *sim*(*RNAi*) animals regenerated photoreceptors with reduced pigmentation (*n*=17/65) and displayed reduced density of the brain neuropil (*n*=30/65; Fig. 5D). Gene knockdown of *arnt* or *sim* resulted in similar regeneration defects and these genes have been shown to interact with each other (Probst et al., 1997). Hence, we also tested the effect of co-silencing *sim* and *arnt*; however, *sim;arnt*(*RNAi*) did not increase the severity of the phenotype above single RNAi treatments (data not shown). The *coe*, *hesl-3* and *sim* knockdown phenotypes, together with the expression of these genes in progenitors and neurons (Figs 1-3), led us to further investigate their potential roles in neuronal regeneration and homeostasis.

Next, we examined the specific roles of *coe*, *hesl-3* and *sim* in nervous system differentiation by evaluating the effect of gene knockdown on the expression of neuronal subtype-specific genes (Fig. 5E-H). We selected the neural marker *ChAT*, which is broadly expressed in the CNS and was co-detected with *coe*$^+$, *hesl-3*$^+$ and *sim*$^+$ cells (Fig. 1J-L), and *cpp-1*, *npp-4* and *npy-2*, which are strongly expressed in neuropeptidergic neurons in the brain (Collins et al., 2010). Using *ChAT* staining we measured the brain area of 7-day regenerates and found that *coe* and *sim* RNAi animals regenerated smaller brains (Fig. 5I). In addition, we observed a significant reduction of *cpp-1*$^+$ cells in *coe*(*RNAi*) animals (Fig. 5F,J) and of *npp-4*$^+$ and *npy-2*$^+$ cells in *coe*(*RNAi*) and *sim*(*RNAi*) animals (Fig. 5F,H,K,L). Furthermore, we observed *ChAT*$^+$, *npy-2*$^+$ and *npp-4*$^+$ cells in aberrant locations following *coe* RNAi (Fig. 5F). Although the brain area difference in *hesl-3*(*RNAi*) regenerates was not statistically significant, we did detect fewer *cpp-1*$^+$, *npp-4*$^+$ and *npy-2*$^+$ neurons (Fig. 5G,I-L). Due to the fact that we observed CNS patterning-like defects in *coe*(*RNAi*) and *hesl-3*(*RNAi*) animals, we tested whether these abnormalities were caused by defects in the stem cells (*smedwi-1*), progeny (*NB.32.1g*, early progeny; *agat-1*, late progeny) or midline signals (*slit* expression) (Cebrià et al., 2007), but we did not find obvious changes in the expression of these markers after *coe* or *hesl-3* RNAi (supplementary material Fig. S8A-C). These data demonstrate that *coe*, *hesl-3* and *sim* are required for expression of neuronal-specific genes and may be necessary for the replacement of neurons following injury. In combination with our expression analyses, these data suggest that *coe*, *hesl-3* and *sim* are expressed in a subset of stem cells committed to neural fates and their function is crucial for neural progenitor maintenance or differentiation.

Development (2013) doi:10.1242/dev.098616

Table 1. Summary of phenotypes observed following RNAi of bHLH homologs in *S. mediterranea*

Gene name	Gene symbol	Phenotype	Developmental role
aryl hydrocarbon receptor	*arh*	Reduced brain neuropil density (14/20)	B-cell and nervous system differentiation
aryl hydrocarbon receptor nuclear translocator	*arnt*	Delayed regeneration and reduced brain neuropil density (12/40)	Differentiation of multiple cell types
atonal homolog 8-1	*atoh8-1*	Delayed regeneration and smaller cg (19/35)	Nervous system differentiation
collier/olfactory-1/early B-cell factor	*coe*	Abnormal pr morphology, flattened morphology, and failure of cg to reconnect (94/114)	B-cell, muscle and nervous system differentiation
daughterless	*da*	Ruffled body margin edges and reduced cg neuropil (70/70)	Neurogenesis, oogenesis and sex determination
hairy and enhancer of split like-3	*hesl-3*	Abnormal pr morphology; single or third pr (20/35)	Negative regulation of Notch signaling
max-interactor-1	*mxi-1*	Abnormal pr morphology (13/40), expanded and disorganized cg (20/40)	Negative regulation of cell proliferation
microphthalmia-associated transcription factor like-1	*mitfl-1*	Lysis (8/40), smaller and disorganized cg (12/40)	Osteoclast differentiation
myc associated factor X	*max*	Lighter pr and smaller cg (15/20)	Negative regulation of gene expression
myogenic differentiation	*myoD*	Failure to regenerate (8/30), abnormal pr morphology; cyclops or bowtie-shaped pr pair (14/30)	Mesoderm specification
single-minded	*sim*	Reduced pr pigmentation (17/65) and cg neuropil density (30/65)	Axon guidance, nervous system differentiation

The number of animals showing the phenotype(s) among the total number examined is indicated in parentheses.
cg, cephalic ganglia; pr, photoreceptor.

Planarians continuously replace cells during normal tissue homeostasis. Therefore, we also assessed the roles of *coe*, *hesl-3* and *sim* in nervous system maintenance by performing extended RNAi treatments (6 weeks) on intact planarians. Knockdown of *hesl-3* and *sim* resulted in no external phenotype or alterations in CNS architecture (data not shown). By contrast, long-term *coe* RNAi resulted in a strong behavioral phenotype in which animals exhibited impaired negative phototaxis and a flattened and stretched body shape with ruffling along the body margin (Fig. 5M; supplementary material Movies 1, 2). Analysis of *ChAT*$^{+}$ and *pc2*$^{+}$ neurons in *coe*(*RNAi*) animals showed that the CNS appeared largely intact except for the absence of *ChAT*$^{+}$ and *pc2*$^{+}$ neurons located at the anterior brain commissure (Fig. 5N). This phenotype was reminiscent of the defect observed in *coe* knockdown regenerates, in which the brain fails to reconnect (Fig. 5B). Because *coe*(*RNAi*) regenerates showed a dramatic reduction of *cpp-1*$^{+}$ brain neurons, we examined whether this cell population was also affected in uninjured *coe*(*RNAi*) animals. Strikingly, we observed an 80% reduction in the number of *cpp-1*$^{+}$ cells in *coe*(*RNAi*) planarians (Fig. 5O,P). Furthermore, when we performed dFISH to *coe* and *cpp-1*, we found that a majority of *cpp-1*$^{+}$ cells also expressed *coe* (81±1.3%; Fig. 5Q). Taken together, our data indicate that *coe* is required for normal function and maintenance of neural tissues and strongly suggest that *cpp-1* may be downstream of *coe*.

DISCUSSION

Although it has been demonstrated that planarians possess pluripotent stem cells (Baguñà et al., 1989; Wagner et al., 2011; Guedelhoefer and Sánchez Alvarado, 2012), several studies support the hypothesis that the stem cell population is heterogeneous (Elliott and Sánchez Alvarado, 2013; Reddien, 2013; Rink, 2013). Analyses of the planarian photoreceptor, excretory and serotonergic cells have shown that tissue-specific transcription factors are detected in the stem cells in intact (Lapan and Reddien, 2012) and regenerating tissues (Lapan and Reddien, 2011; Scimone et al., 2011; Currie and Pearson, 2013); these studies have identified the first sets of precursor cells in planarians outside of the germ cells (Newmark et al., 2008) and have generated a working model in which planarians possess diverse lineage-committed progenitors that contribute to the maintenance and regeneration of tissues (Reddien, 2013; Rink, 2013). In contrast to the well-defined excretory system and photoreceptors, the nervous system represents a formidable challenge. At the molecular level, there are potentially dozens of neuronal subtypes (Cebrià, 2007; Collins et al., 2010; Gentile et al., 2011; Umesono et al., 2011), and it is largely unknown whether the generation of neural diversity is solely dependent on the pluripotent stem cells or lineage-restricted progenitors. In our study, we investigated this question by analyzing the bHLH gene family. By combining *in situ* hybridization analyses and RNAi studies, we identified nine bHLH genes expressed in specific neural and stem cell subpopulations that were required for regeneration (Fig. 6A), which strongly suggested that these phenotypes could be due to abnormal neural differentiation and/or function.

Identification of neuronal progenitor cells in planarians

Owing to the mRNA expression in stem cells and neurons, we focused our analyses on *coe*, *hesl-3* and *sim*, which are known to serve major roles in neurogenesis in both vertebrate and invertebrate organisms (Dubois and Vincent, 2001; Kewley et al., 2004; Kageyama et al., 2008). As we expected, using BrdU, we observed *coe*, *hesl-3* and *sim* expression in cycling stem cells located in the mesenchyme of intact animals. Over the course of 48 hours, we observed an increase in the proportion of BrdU^{+} cells that expressed *coe* and *sim* and detected many of these cells in the cephalic ganglia. We hypothesize that the observed increase in the proportion of BrdU^{+}/*coe*$^{+}$ and BrdU^{+}/*sim*$^{+}$ cells over time is from both progenitors that maintain expression of *coe* or *sim* as they divide and begin to differentiate and additional cells that turn on expression of these genes during differentiation. Additionally, the increase in the proportion of double-labeled cells could also be accounted for by a contribution of newly generated progenitor cells. Together with the observation that the number of *coe*$^{+}$ and *sim*$^{+}$ cells increases following induction of ectopic neurogenesis and the requirement of *coe* and *sim* during CNS regeneration (RNAi studies discussed below), our data suggest that a subset of *coe*- and *sim*-expressing cells represent multipotent neural progenitors (Fig. 6B). We propose that these *coe*$^{+}$ and *sim*$^{+}$ progenitors migrate and terminally differentiate in the CNS. By contrast, we did not observe an increase

Development (2013) doi:10.1242/dev.098616

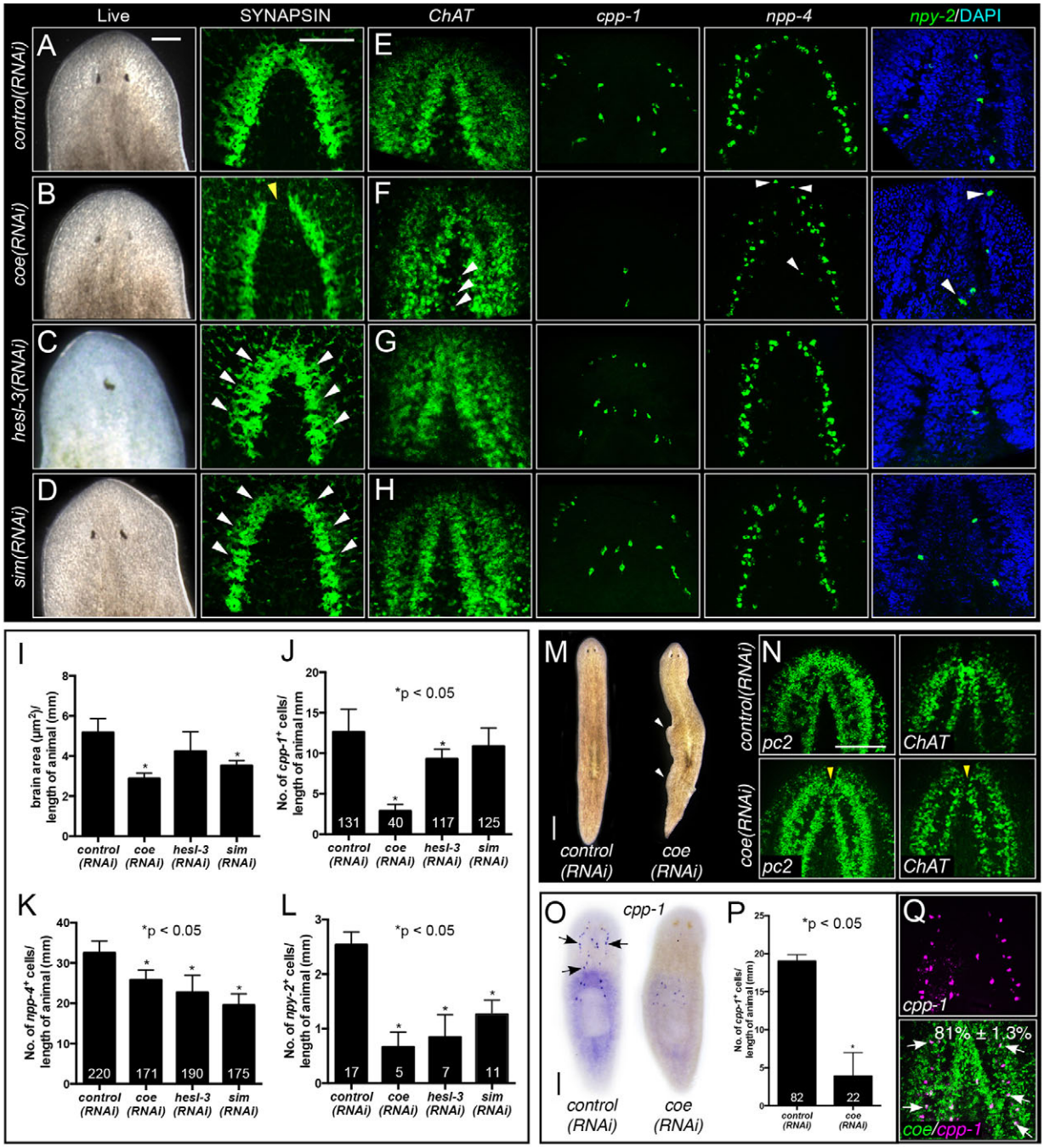

Fig. 5. *coe*, *hesl-3* and *sim* are required for CNS regeneration. (A-D) Images of live or immunostained RNAi-treated animals after 10 days of regeneration. The yellow arrowhead in B marks a commissure defect, and white arrowheads in C and D mark the abnormal brain morphology and a dramatic reduction of neuropil density observed in *hesl-3* and *sim* RNAi planarians, respectively. (E-H) Seven days following amputation, RNAi animals were processed for FISH to *ChAT*, *cpp-1*, *npp-4* or *npy-2* (n=20). Arrowheads in F denote aberrant location of *npp-4*$^+$ and *npy-2*$^+$ neurons (the latter were counterstained with DAPI to visualize the brain). (I-L) Quantification of neurons shown in E-H; the total number of cells counted are indicated within each bar. (M-O) After 24 days of RNAi treatment uninjured control and *coe*(*RNAi*) animals were imaged live (M) or processed for FISH to *pc2* or *ChAT* (N; n=10) or WISH to *cpp-1* (O; n=15). (P) Quantification of *cpp-1*$^+$ cells in O. (Q) FISH to *cpp-1* and *coe*, and quantification of *cpp-1*$^+$ cells that also expressed *coe*. Scale bars: 100 μm.

in the proportion of BrdU$^+$/*hesl-3*$^+$ cells near the brain; it is possible that *hesl-3* expression is downregulated during cell-fate specification and that this gene may be regulating progenitor maintenance or the timing of neural stem cell differentiation, scenarios that are consistent with known roles of HES genes (Hatakeyama et al., 2004; Kageyama et al., 2008). Although some *coe*$^+$ and *sim*$^+$ cells were observed in the posterior end of the animal, neural progenitors were most prevalent in the area anterior to the pharynx and posterior to the base of the brain, the location where eye progenitors (*ovo*$^+$/*smedwi-1*$^+$ cells) were also detected (Lapan and Reddien, 2012). Interestingly, our observation that the proportion of BrdU$^+$/*coe*$^+$ and BrdU$^+$/*sim*$^+$ cells located in the pre-pharyngeal area increased over time suggests that this area may represent a ‘neurogenic zone’ in planarians. Our data support a model in which

Development (2013) doi:10.1242/dev.098616

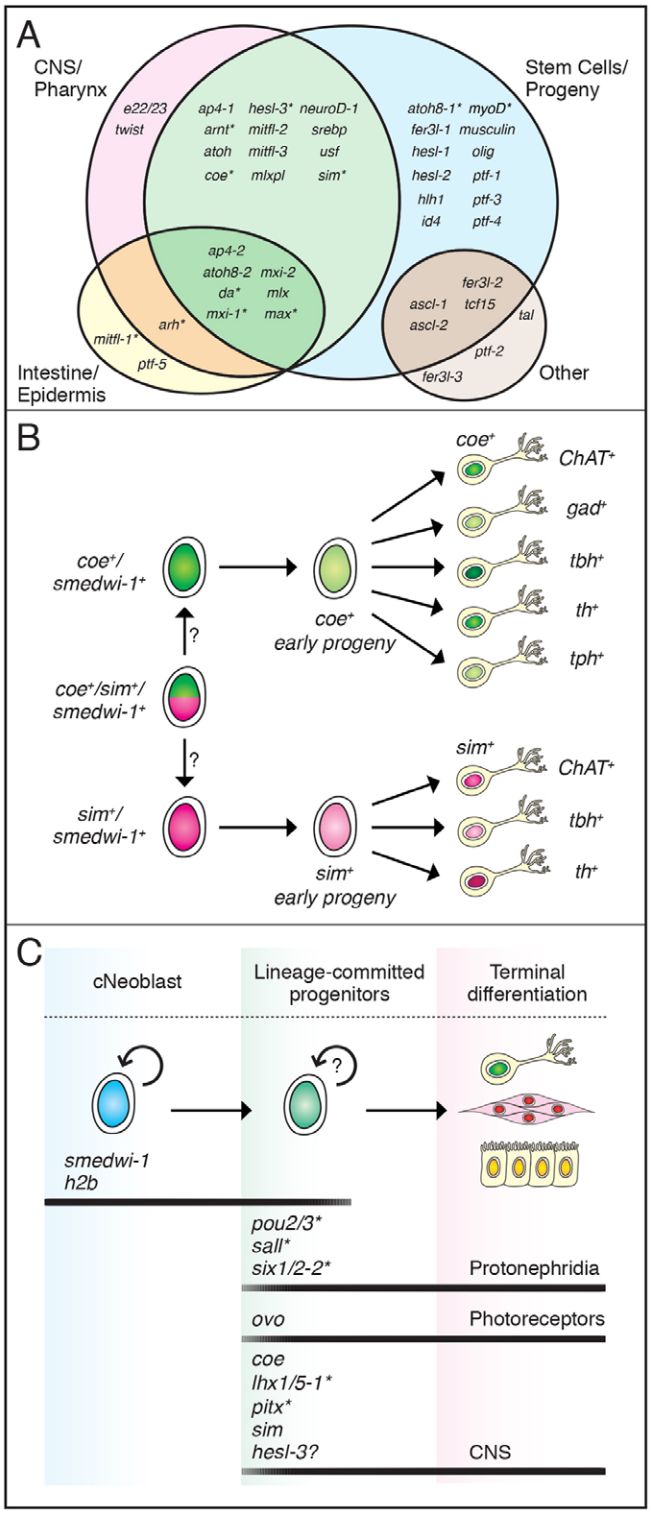

Fig. 6. Planarians possess lineage-committed neural progenitors. (A) Venn diagram summarizing genome-wide expression and functional analysis of bHLH genes in planarians. *Regeneration defects were observed following RNAi. (B) Model of *coe*$^+$ and *sim*$^+$ progenitor cell differentiation into specific neural subtypes. (C) Model of cell differentiation in planarians. Pluripotent adult stem cells (cNeoblasts; *smedwi-1*$^+$ and *h2b*$^+$) have the ability to self-renew and generate lineage-committed progenitors. Summary of identified genes marking photoreceptor (Lapan and Reddien, 2012), protonephridia (Scimone et al., 2011), serotonergic (Currie and Pearson, 2013) and novel CNS (bHLH) progenitors, respectively. *Progenitors that are only observed during regeneration.

pluripotent stem cells (cNeoblasts) maintain lineage-committed progenitors, which generate most if not all of the cells required to meet normal physiological demands in uninjured planarians (Fig. 6C).

bHLH genes with roles in planarian CNS regeneration

Planarians possess members from all of the families of proneural factors, including homologs of *acheate-scute*, *atonal*, *neuroD* and *da*, all of which are primarily expressed in the stem cells. With the exception of *atoh8-1* RNAi, which caused animals to regenerate smaller brains, we found that gene knockdown of most proneural homologs failed to cause overt regeneration defects, even after long-term or combinatorial RNAi. Nonetheless, we did find that co-silencing of *ascl-1* or *neuroD-1* together with *ndk* suppressed ectopic formation of *npp-4*$^+$ neurons. We surmise that knockdown of some bHLHs may cause subtle defects in neural specification, which are difficult to detect with the use of pan-neural markers. Future functional studies using discrete nervous system markers may reveal additional roles of bHLH genes in CNS differentiation.

On the bases of gene expression patterns and RNAi phenotypes, we further explored the function of *coe*, *hesl-3* and *sim*. *coe* genes are conserved in metazoans and are known to play roles in neuronal specification, migration, axon guidance, dendritogenesis, neuronal subtype specification (Wightman et al., 1997; Dubois et al., 1998; Prasad et al., 1998; Garel et al., 2000; Pozzoli et al., 2001; Garcia-Dominguez et al., 2003; Hattori et al., 2007; Jinushi-Nakao et al., 2007; Crozatier and Vincent, 2008; Demilly et al., 2011; Kratsios et al., 2012), and cellular reprogramming (Richard et al., 2011). In planarians, *coe* knockdown led to a failure of animals to connect the cephalic ganglia. Analysis of this defect using neural subtype markers showed that neurons were found in aberrant locations. In addition, long-term silencing caused animals to exhibit abnormal locomotion and decreases of cholinergic and *pc2*$^+$ neurons at the anterior commissure and brain *cpp-1*$^+$ neurons. In *C. elegans*, *coe* (*unc-3*) mutants exhibit behavioral abnormalities (Wightman et al., 1997), a defect that is caused by a loss of cholinergic motoneuron properties (Kratsios et al., 2012). Our data show that *coe* is playing a conserved role in neuronal differentiation during both CNS regeneration and maintenance. *coe* homologs in humans (EBF transcription factors) have been associated with cancers of the nervous system (Liao, 2009), yet the genetic targets of *coe* homologs have not been fully characterized. Thus, further investigation of *coe* function in planarians may reveal mechanisms regulating neural progenitor populations.

hes genes are a primary target of Notch signaling and defects in *hes* genes cause premature neural differentiation and depletion of the neural progenitor pool in mice (Ishibashi et al., 1995; Kageyama et al., 2008). In planarians, *hesl-3* knockdown led animals to regenerate mispatterned brains and a reduction of *cpp-1*$^+$, *npp-4*$^+$ and *npy-2*$^+$ brain neurons. These data suggest *hesl-3* plays a role in neural fate regulation during CNS repair. At present, the role of Notch signaling in planarians has not been extensively characterized. Thus, analysis of *hesl* genes in stem cell regulation should be a focus of future investigations.

Finally, in flies and crustaceans, *sim* functions as a master regulator of midline cells by regulating the specification of midline progenitors (Nambu et al., 1991; Vargas-Vila et al., 2010), whereas in vertebrates, *sim* controls the differentiation (Michaud et al., 1998; Eaton and Glasgow, 2006) and migration (via plexinC1) (Xu and Fan, 2007) of certain neuroendocrine lineages. *sim* does not appear to function as a master regulator of the midline in planarians. However, *sim* RNAi caused animals to regenerate smaller brains

with fewer *npp-4*$^+$ and *npy-2*$^+$ neurons, suggesting a potential role in specification and/or guidance of cells from the neuroendocrine lineage. To further explore this possibility, future experiments should test the effects of *sim* knockdown on the fate of all neuropeptide-expressing neurons (Collins et al., 2010) or the expression of guidance molecules, such as plexin homologs.

Conclusions

Our work has revealed that planarians possess lineage-committed progenitors that contribute to the maintenance and regeneration of the CNS. We also identified nine bHLH genes that regulate adult neurogenesis and are required for nervous system repair. This study sets the stage to use planarians as a model to elucidate roles of bHLH genes in adult pluripotent stem cell differentiation. Furthermore, by extending our analysis of bHLH factors genome-wide, this study will serve as a resource for future investigation into bHLH evolution and function.

MATERIALS AND METHODS

Animals

Asexual *Schmidtea mediterranea* (CIW4) were maintained as previously described (Cebrià and Newmark, 2005). Animals 2-5 mm in length that were starved for 1 week were used for all experiments.

bHLH identification, phylogenetic analysis and cloning

To identify planarian bHLH genes, TBLASTN searches were performed against the *S. mediterranea* genome (Robb et al., 2008) and several transcriptomes (Zayas et al., 2005; Adamidi et al., 2011; Labbé et al., 2012; Önal et al., 2012) using bHLH protein sequences from human, mouse and fly. Putative planarian bHLH homologs were validated by performing reciprocal BLASTX against the nr database (NCBI). The bHLH superfamily consists of six monophyletic groups (Groups A-F), which are also characterized by the presence or absence of various additional protein domains (Simionato et al., 2007). Due to the large number of putative paralogs in Groups A and B, the predicted protein sequences were aligned using T-Coffee (Notredame et al., 2000) and subjected to Bayesian analyses as described previously (Currie and Pearson, 2013; Zhu and Pearson, 2013); Group C-F genes were categorized based on clear top BLASTP hits against the Swiss-Prot database (UniProt) and the presence of class-specific protein domains (supplementary material Table S1). bHLH sequences were obtained from a cDNA collection (Zayas et al., 2005) or cloned from cDNA into pJC53.2 (Collins et al., 2010) or pPR244 (Reddien et al., 2005a) using gene specific primers or 3′ RACE, respectively. bHLH sequences were deposited in GenBank. The primers used and GenBank accession numbers are listed in supplementary material Table S2.

In situ hybridization

Riboprobes were synthesized and animals were processed for *in situ* hybridization as previously described (Pearson et al., 2009). For γ-irradiation treatments, animals were exposed to 100 Gy in a JL Shepherd Mark I Cesium-137 irradiator and fixed 6 days after treatment. To visualize bHLH transcripts by multiple fluorescent *in situ* hybridization (FISH), we used horseradish peroxidase substrates as described previously (Pearson et al., 2009) or the alkaline phosphatase (AP) substrate Fast Blue (Lauter et al., 2011; Currie and Pearson, 2013). For Fast Blue staining, animals were developed in 0.25 mg/ml Fast Blue BB (Sigma F3378) and NAMP (Sigma 855) in AP staining buffer (0.1 M Tris-HCl pH 8.2, containing 50 mM $MgCl_2$, 100 mM NaCl, 0.1% Tween 20) (Hauptmann, 2001; Lauter et al., 2011).

BrdU staining

Experiments were conducted by soaking animals in BrdU for 1 hour as previously described (Cowles et al., 2012), chasing for 4, 24 or 48 hours before fixation and processing for FISH, and then processing for BrdU labeling starting with the HCl treatment.

RNA interference

For regeneration studies, we administered six feedings of bacterially expressed dsRNA over 3 weeks as previously described (Gurley et al, 2008). *gfp* was used as a control for all experiments. 24 hours following the final RNAi treatment, animals were amputated anterior to the pharynx, observed for 10 days and then processed for *in situ* hybridization or immunostaining. For long-term experiments, animals were fed 12 times over 6 weeks before amputation; uninjured animals were fixed 1 week after the final feeding. Relative gene expression after RNAi was determined by real-time quantitative PCR as described previously (Hubert et al., 2013); primers are listed in supplementary material Table S2.

Immunohistochemistry

Immunostaining with anti-SYNAPSIN (1:400, 3C10, Developmental Studies Hybridoma Bank) and anti-phosphohistone-H3 (S10) (1:1000, D2C8, Cell Signaling) were performed as previously described (Cowles et al., 2012).

Imaging

Images were acquired using a Leica DFC450 camera mounted on a Leica M205 stereomicroscope. Animals labeled with fluorescent probes were imaged with an Axiocam MRm camera mounted on a Zeiss SteREO Lumar V.12 or Axio Observer.Z1 equipped with an ApoTome, or a Hamamatsu ImagEM C9100-13 camera mounted on an Olympus IX81 microscope equipped with a Yokogawa CSU X1 spinning-disk confocal scan head.

Cell counting

Ten 1-µm optical sections were captured from selected regions and merged, and cells were hand-counted using ImageJ 1.43u software. The proportions of cells co-expressing specific neurotransmitters or *smedwi-1* and *coe*, *hesl-3* or *sim* were calculated from >100 cells counted from three to five animals. The proportion of BrdU$^+$ cells co-expressing specific genes was calculated from >300 BrdU$^+$ cells counted from three to five animals. For analysis of *ndk* RNAi animals, *coe*$^+$ and *sim*$^+$ cells were counted and normalized per mm^3; ectopic *npp-4*$^+$ cells were counted from the posterior end of the brain to the posterior boundary of the pharynx and normalized to the length of the animal. Mean and s.d. values were computed and statistical comparisons were performed using an unpaired Student's *t*-test. Error bars in graphs are s.d.

Acknowledgements

We thank Jordana Henderson, Amy Hubert and Kelly Ross for helpful comments on the manuscript, Kayla Muth for assistance with RNAi experiments, Claire Cowles for artwork design, and the anonymous reviewers whose constructive criticisms improved this work.

Competing interests

The authors declare no competing financial interests.

Author contributions

M.W.C. and R.M.Z. designed and interpreted the experiments and wrote the manuscript. M.W.C., D.D.R.B., S.V.N. and B.N.S. conducted the experiments and analyzed the data. B.J.P. performed phylogenetic analysis. M.W.C, B.J.P. and R.M.Z. discussed the results and edited the final version of the manuscript.

Funding

M.W.C. acknowledges support from the San Diego Chapter of the Achievement Rewards for College Scientists Foundation and the Inamori Foundation. D.D.R.B. was supported by a Canadian Institutes of Health Research Student Fellowship [GSD-121763]. This research was supported by a Natural Sciences and Engineering Research Council of Canada grant [402264-11] and Ontario Institute for Cancer Research New Investigator Award [IA-026] to B.J.P. and a California Institute for Regenerative Medicine grant [RN2-00940-1] to R.M.Z.

Supplementary material

Supplementary material available online at
http://dev.biologists.org/lookup/suppl/doi:10.1242/dev.098616/-/DC1

References

Adamidi, C., Wang, Y., Gruen, D., Mastrobuoni, G., You, X., Tolle, D., Dodt, M., Mackowiak, S. D., Gogol-Doering, A., Oenal, P. et al. (2011). De novo assembly

and validation of planaria transcriptome by massive parallel sequencing and shotgun proteomics. *Genome Res.* **21**, 1193-1200.
Baguñà, J. (2012). The planarian neoblast: the rambling history of its origin and some current black boxes. *Int. J. Dev. Biol.* **56**, 19-37.
Baguñà, J., Saló, E. and Auladell, C. (1989). Regeneration and pattern formation in planarians. III. Evidence that neoblasts are totipotent stem cells and the source of blastema cells. *Development* **107**, 77-86.
Bertrand, N., Castro, D. S. and Guillemot, F. (2002). Proneural genes and the specification of neural cell types. *Nat. Rev. Neurosci.* **3**, 517-530.
Blassberg, R. A., Felix, D. A., Tejada-Romero, B. and Aboobaker, A. A. (2013). PBX/extradenticle is required to re-establish axial structures and polarity during planarian regeneration. *Development* **140**, 730-739.
Bullock, T. H. and Horridge, G. A. (1965). *Structure and Function in the Nervous Systems of Invertebrates*. San Francisco, CA, USA: W. H. Freeman.
Cebrià, F. (2007). Regenerating the central nervous system: how easy for planarians! *Dev. Genes Evol.* **217**, 733-748.
Cebrià, F. and Newmark, P. A. (2005). Planarian homologs of netrin and netrin receptor are required for proper regeneration of the central nervous system and the maintenance of nervous system architecture. *Development* **132**, 3691-3703.
Cebrià, F., Kobayashi, C., Umesono, Y., Nakazawa, M., Mineta, K., Ikeo, K., Gojobori, T., Itoh, M., Taira, M., Sánchez Alvarado, A. et al. (2002). FGFR-related gene nou-darake restricts brain tissues to the head region of planarians. *Nature* **419**, 620-624.
Cebrià, F., Guo, T., Jopek, J. and Newmark, P. A. (2007). Regeneration and maintenance of the planarian midline is regulated by a slit orthologue. *Dev. Biol.* **307**, 394-406.
Collins, J. J., 3rd, Hou, X., Romanova, E. V., Lambrus, B. G., Miller, C. M., Saberi, A., Sweedler, J. V. and Newmark, P. A. (2010). Genome-wide analyses reveal a role for peptide hormones in planarian germline development. *PLoS Biol.* **8**, e1000509.
Cowles, M. W., Hubert, A. and Zayas, R. M. (2012). A Lissencephaly-1 homologue is essential for mitotic progression in the planarian Schmidtea mediterranea. *Dev. Dyn.* **241**, 901-910.
Crozatier, M. and Vincent, A. (2008). Control of multidendritic neuron differentiation in Drosophila: the role of Collier. *Dev. Biol.* **315**, 232-242.
Currie, K. W. and Pearson, B. J. (2013). Transcription factors lhx1/5-1 and pitx are required for the maintenance and regeneration of serotonergic neurons in planarians. *Development* **140**, 3577-3588.
Demilly, A., Simionato, E., Ohayon, D., Kerner, P., Garcès, A. and Vervoort, M. (2011). Coe genes are expressed in differentiating neurons in the central nervous system of protostomes. *PLoS ONE* **6**, e21213.
Dubois, L. and Vincent, A. (2001). The COE–Collier/Olf1/EBF–transcription factors: structural conservation and diversity of developmental functions. *Mech. Dev.* **108**, 3-12.
Dubois, L., Bally-Cuif, L., Crozatier, M., Moreau, J., Paquereau, L. and Vincent, A. (1998). XCoe2, a transcription factor of the Col/Olf-1/EBF family involved in the specification of primary neurons in Xenopus. *Curr. Biol.* **8**, 199-209.
Eaton, J. L. and Glasgow, E. (2006). The zebrafish bHLH PAS transcriptional regulator, single-minded 1 (sim1), is required for isotocin cell development. *Dev. Dyn.* **235**, 2071-2082.
Eisenhoffer, G. T., Kang, H. and Sánchez Alvarado, A. (2008). Molecular analysis of stem cells and their descendants during cell turnover and regeneration in the planarian Schmidtea mediterranea. *Cell Stem Cell* **3**, 327-339.
Elliott, S. A. and Sánchez Alvarado, A. (2013). The history and enduring contributions of planarians to the study of animal regeneration. *Wiley Interdiscip. Rev. Dev. Biol.* **2**, 301-326.
Felix, D. A. and Aboobaker, A. A. (2010). The TALE class homeobox gene Smed-prep defines the anterior compartment for head regeneration. *PLoS Genet.* **6**, e1000915.
Forsthoefel, D. J., Park, A. E. and Newmark, P. A. (2011). Stem cell-based growth, regeneration, and remodeling of the planarian intestine. *Dev. Biol.* **356**, 445-459.
Forsthoefel, D. J., James, N. P., Escobar, D. J., Stary, J. M., Vieira, A. P., Waters, F. A. and Newmark, P. A. (2012). An RNAi screen reveals intestinal regulators of branching morphogenesis, differentiation, and stem cell proliferation in planarians. *Dev. Cell* **23**, 691-704.
Gage, F. H. (2002). Neurogenesis in the adult brain. *J. Neurosci.* **22**, 612-613.
Galliot, B., Quiquand, M., Ghila, L., de Rosa, R., Miljkovic-Licina, M. and Chera, S. (2009). Origins of neurogenesis, a cnidarian view. *Dev. Biol.* **332**, 2-24.
Garcia-Dominguez, M., Poquet, C., Garel, S. and Charnay, P. (2003). Ebf gene function is required for coupling neuronal differentiation and cell cycle exit. *Development* **130**, 6013-6025.
Garel, S., Garcia-Dominguez, M. and Charnay, P. (2000). Control of the migratory pathway of facial branchiomotor neurones. *Development* **127**, 5297-5307.
Gentile, L., Cebrià, F. and Bartscherer, K. (2011). The planarian flatworm: an in vivo model for stem cell biology and nervous system regeneration. *Dis. Model. Mech.* **4**, 12-19.
Goulding, S. E., zur Lage, P. and Jarman, A. P. (2000). amos, a proneural gene for Drosophila olfactory sense organs that is regulated by lozenge. *Neuron* **25**, 69-78.
Guedelhoefer, O. C., 4th and Sánchez Alvarado, A. (2012). Amputation induces stem cell mobilization to sites of injury during planarian regeneration. *Development* **139**, 3510-3520.
Guillemot, F. (2007). Spatial and temporal specification of neural fates by transcription factor codes. *Development* **134**, 3771-3780.
Gurley, K. A., Rink, J. C. and Sánchez Alvarado, A. (2008). Beta-catenin defines head versus tail identity during planarian regeneration and homeostasis. *Science* **319**, 323-327.
Hatakeyama, J., Bessho, Y., Katoh, K., Ookawara, S., Fujioka, M., Guillemot, F. and Kageyama, R. (2004). Hes genes regulate size, shape and histogenesis of the nervous system by control of the timing of neural stem cell differentiation. *Development* **131**, 5539-5550.
Hattori, Y., Sugimura, K. and Uemura, T. (2007). Selective expression of Knot/Collier, a transcriptional regulator of the EBF/Olf-1 family, endows the Drosophila sensory system with neuronal class-specific elaborated dendritic patterns. *Genes Cells* **12**, 1011-1022.
Hauptmann, G. (2001). One-, two-, and three-color whole-mount in situ hybridization to Drosophila embryos. *Methods* **23**, 359-372.
Huang, M. L., Hsu, C. H. and Chien, C. T. (2000). The proneural gene amos promotes multiple dendritic neuron formation in the Drosophila peripheral nervous system. *Neuron* **25**, 57-67.
Hubert, A., Henderson, J. M., Ross, K. G., Cowles, M. W., Torres, J. and Zayas, R. M. (2013). Epigenetic regulation of planarian stem cells by the SET1/MLL family of histone methyltransferases. *Epigenetics* **8**, 79-91.
Iglesias, M., Almuedo-Castillo, M., Aboobaker, A. A. and Saló, E. (2011). Early planarian brain regeneration is independent of blastema polarity mediated by the Wnt/β-catenin pathway. *Dev. Biol.* **358**, 68-78.
Ishibashi, M., Ang, S. L., Shiota, K., Nakanishi, S., Kageyama, R. and Guillemot, F. (1995). Targeted disruption of mammalian hairy and Enhancer of split homolog-1 (HES-1) leads to up-regulation of neural helix-loop-helix factors, premature neurogenesis, and severe neural tube defects. *Genes Dev.* **9**, 3136-3148.
Jan, Y. N. and Jan, L. Y. (1994). Neuronal cell fate specification in Drosophila. *Curr. Opin. Neurobiol.* **4**, 8-13.
Jinushi-Nakao, S., Arvind, R., Amikura, R., Kinameri, E., Liu, A. W. and Moore, A. W. (2007). Knot/Collier and cut control different aspects of dendrite cytoskeleton and synergize to define final arbor shape. *Neuron* **56**, 963-978.
Kageyama, R., Ohtsuka, T. and Kobayashi, T. (2008). Roles of Hes genes in neural development. *Dev. Growth Differ.* **50** Suppl., S97-S103.
Kempermann, G. (2011). *Adult Neurogenesis*. New York, NY, USA: Oxford University Press.
Kempermann, G. (2012). New neurons for 'survival of the fittest'. *Nat. Rev. Neurosci.* **13**, 727-736.
Kewley, R. J., Whitelaw, M. L. and Chapman-Smith, A. (2004). The mammalian basic helix-loop-helix/PAS family of transcriptional regulators. *Int. J. Biochem. Cell Biol.* **36**, 189-204.
King, R. S. and Newmark, P. A. (2012). The cell biology of regeneration. *J. Cell Biol.* **196**, 553-562.
Kintner, C. (2002). Neurogenesis in embryos and in adult neural stem cells. *J. Neurosci.* **22**, 639-643.
Kratsios, P., Stolfi, A., Levine, M. and Hobert, O. (2012). Coordinated regulation of cholinergic motor neuron traits through a conserved terminal selector gene. *Nat. Neurosci.* **15**, 205-214.
Kretzschmar, K. and Watt, F. M. (2012). Lineage tracing. *Cell* **148**, 33-45.
Labbé, R. M., Irimia, M., Currie, K. W., Lin, A., Zhu, S. J., Brown, D. D., Ross, E. J., Voisin, V., Bader, G. D., Blencowe, B. J. et al. (2012). A comparative transcriptomic analysis reveals conserved features of stem cell pluripotency in planarians and mammals. *Stem Cells* **30**, 1734-1745.
Lapan, S. W. and Reddien, P. W. (2011). dlx and sp6-9 Control optic cup regeneration in a prototypic eye. *PLoS Genet.* **7**, e1002226.
Lapan, S. W. and Reddien, P. W. (2012). Transcriptome analysis of the planarian eye identifies ovo as a specific regulator of eye regeneration. *Cell Rep.* **2**, 294-307.
Lauter, G., Söll, I. and Hauptmann, G. (2011). Two-color fluorescent in situ hybridization in the embryonic zebrafish brain using differential detection systems. *BMC Dev. Biol.* **11**, 43.
Lentz, T. L. (1968). *Primitive Nervous Systems*. New Haven, CT, USA: Yale University Press.
Liao, D. (2009). Emerging roles of the EBF family of transcription factors in tumor suppression. *Mol. Cancer Res.* **7**, 1893-1901.
Lindsey, B. W. and Tropepe, V. (2006). A comparative framework for understanding the biological principles of adult neurogenesis. *Prog. Neurobiol.* **80**, 281-307.
Michaud, J. L., Rosenquist, T., May, N. R. and Fan, C. M. (1998). Development of neuroendocrine lineages requires the bHLH-PAS transcription factor SIM1. *Genes Dev.* **12**, 3264-3275.
Nambu, J. R., Lewis, J. O., Wharton, K. A., Jr and Crews, S. T. (1991). The Drosophila single-minded gene encodes a helix-loop-helix protein that acts as a master regulator of CNS midline development. *Cell* **67**, 1157-1167.
Newmark, P. A. and Sánchez Alvarado, A. (2000). Bromodeoxyuridine specifically labels the regenerative stem cells of planarians. *Dev. Biol.* **220**, 142-153.
Newmark, P. A., Wang, Y. and Chong, T. (2008). Germ cell specification and regeneration in planarians. *Cold Spring Harb. Symp. Quant. Biol.* **73**, 573-581.
Notredame, C., Higgins, D. G. and Heringa, J. (2000). T-Coffee: a novel method for fast and accurate multiple sequence alignment. *J. Mol. Biol.* **302**, 205-217.
Önal, P., Grün, D., Adamidi, C., Rybak, A., Solana, J., Mastrobuoni, G., Wang, Y., Rahn, H. P., Chen, W., Kempa, S. et al. (2012). Gene expression of pluripotency determinants is conserved between mammalian and planarian stem cells. *EMBO J.* **31**, 2755-2769.
Pearson, B. J., Eisenhoffer, G. T., Gurley, K. A., Rink, J. C., Miller, D. E. and Sánchez Alvarado, A. (2009). Formaldehyde-based whole-mount in situ hybridization method for planarians. *Dev. Dyn.* **238**, 443-450.

Pozzoli, O., Bosetti, A., Croci, L., Consalez, G. G. and Vetter, M. L. (2001). Xebf3 is a regulator of neuronal differentiation during primary neurogenesis in Xenopus. *Dev. Biol.* **233**, 495-512.

Prasad, B. C., Ye, B., Zackhary, R., Schrader, K., Seydoux, G. and Reed, R. R. (1998). unc-3, a gene required for axonal guidance in Caenorhabditis elegans, encodes a member of the O/E family of transcription factors. *Development* **125**, 1561-1568.

Probst, M. R., Fan, C. M., Tessier-Lavigne, M. and Hankinson, O. (1997). Two murine homologs of the Drosophila single-minded protein that interact with the mouse aryl hydrocarbon receptor nuclear translocator protein. *J. Biol. Chem.* **272**, 4451-4457.

Ramón y Cajal, S. (1928). *Degeneration and Regeneration of the Nervous System*. London, UK: Oxford University Press.

Reddien, P. W. (2013). Specialized progenitors and regeneration. *Development* **140**, 951-957.

Reddien, P. W., Bermange, A. L., Murfitt, K. J., Jennings, J. R. and Sánchez Alvarado, A. (2005a). Identification of genes needed for regeneration, stem cell function, and tissue homeostasis by systematic gene perturbation in planaria. *Dev. Cell* **8**, 635-649.

Reddien, P. W., Oviedo, N. J., Jennings, J. R., Jenkin, J. C. and Sánchez Alvarado, A. (2005b). SMEDWI-2 is a PIWI-like protein that regulates planarian stem cells. *Science* **310**, 1327-1330.

Resch, A. M., Palakodeti, D., Lu, Y. C., Horowitz, M. and Graveley, B. R. (2012). Transcriptome analysis reveals strain-specific and conserved stemness genes in Schmidtea mediterranea. *PLoS ONE* **7**, e34447.

Richard, J. P., Zuryn, S., Fischer, N., Pavet, V., Vaucamps, N. and Jarriault, S. (2011). Direct in vivo cellular reprogramming involves transition through discrete, non-pluripotent steps. *Development* **138**, 1483-1492.

Richards, G. S., Simionato, E., Perron, M., Adamska, M., Vervoort, M. and Degnan, B. M. (2008). Sponge genes provide new insight into the evolutionary origin of the neurogenic circuit. *Curr. Biol.* **18**, 1156-1161.

Rink, J. C. (2013). Stem cell systems and regeneration in planaria. *Dev. Genes Evol.* **223**, 67-84.

Robb, S. M., Ross, E. and Sánchez Alvarado, A. (2008). SmedGD: the Schmidtea mediterranea genome database. *Nucleic Acids Res.* **36**, D599-D606.

Scimone, M. L., Srivastava, M., Bell, G. W. and Reddien, P. W. (2011). A regulatory program for excretory system regeneration in planarians. *Development* **138**, 4387-4398.

Simionato, E., Ledent, V., Richards, G., Thomas-Chollier, M., Kerner, P., Coornaert, D., Degnan, B. M. and Vervoort, M. (2007). Origin and diversification of the basic helix-loop-helix gene family in metazoans: insights from comparative genomics. *BMC Evol. Biol.* **7**, 33.

Solana, J., Kao, D., Mihaylova, Y., Jaber-Hijazi, F., Malla, S., Wilson, R. and Aboobaker, A. (2012). Defining the molecular profile of planarian pluripotent stem cells using a combinatorial RNAseq, RNA interference and irradiation approach. *Genome Biol.* **13**, R19.

Umesono, Y., Tasaki, J., Nishimura, K., Inoue, T. and Agata, K. (2011). Regeneration in an evolutionarily primitive brain–the planarian Dugesia japonica model. *Eur. J. Neurosci.* **34**, 863-869.

Vargas-Vila, M. A., Hannibal, R. L., Parchem, R. J., Liu, P. Z. and Patel, N. H. (2010). A prominent requirement for single-minded and the ventral midline in patterning the dorsoventral axis of the crustacean Parhyale hawaiensis. *Development* **137**, 3469-3476.

Wagner, D. E., Wang, I. E. and Reddien, P. W. (2011). Clonogenic neoblasts are pluripotent adult stem cells that underlie planarian regeneration. *Science* **332**, 811-816.

Wightman, B., Baran, R. and Garriga, G. (1997). Genes that guide growth cones along the C. elegans ventral nerve cord. *Development* **124**, 2571-2580.

Xu, C. and Fan, C. M. (2007). Allocation of paraventricular and supraoptic neurons requires Sim1 function: a role for a Sim1 downstream gene PlexinC1. *Mol. Endocrinol.* **21**, 1234-1245.

Zayas, R. M., Hernández, A., Habermann, B., Wang, Y., Stary, J. M. and Newmark, P. A. (2005). The planarian Schmidtea mediterranea as a model for epigenetic germ cell specification: analysis of ESTs from the hermaphroditic strain. *Proc. Natl. Acad. Sci. USA* **102**, 18491-18496.

Zhu, S. J. and Pearson, B. J. (2013). The Retinoblastoma pathway regulates stem cell proliferation in freshwater planarians. *Dev. Biol.* **373**, 442-452.

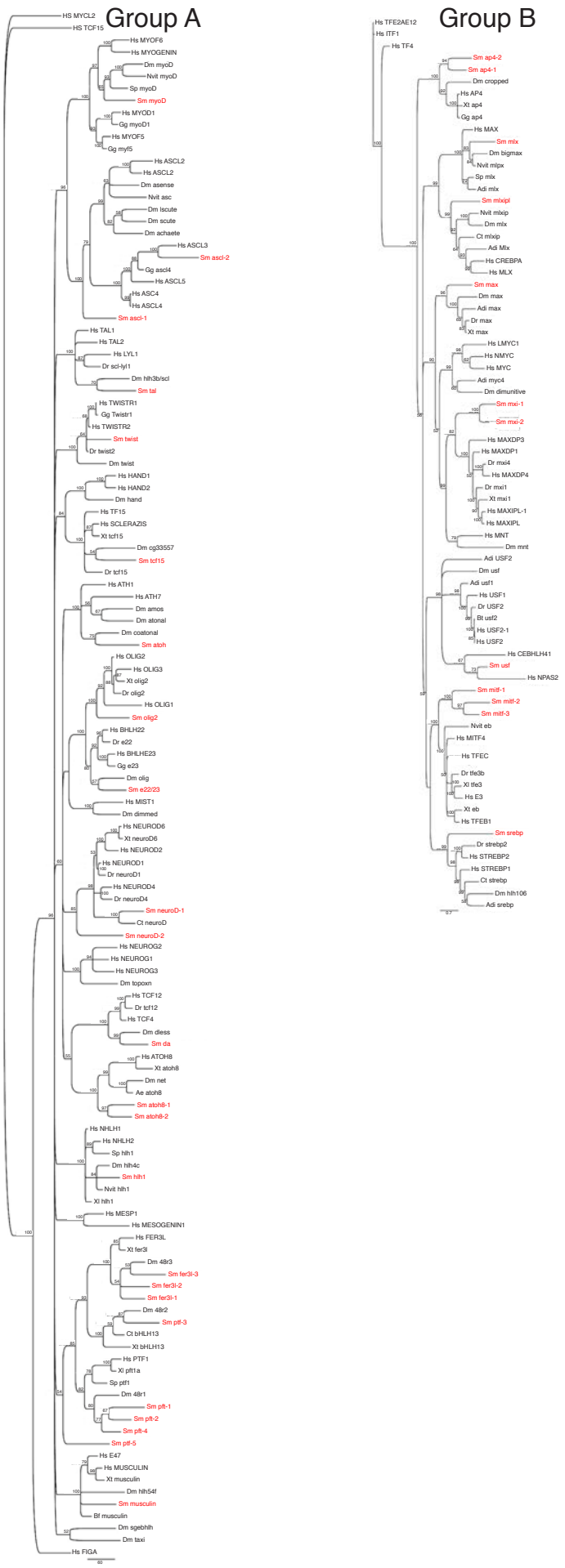

Fig. S1: Bayesian Phylogeny of Groups A and B bHLH transcription factor homologs. Protein sequences used in the phylogenies were obtained from the NCBI Entrez protein database or directly from the genome sequencing projects of included organisms. Sequences were aligned using T-Coffee (Notredame et al., 2000) and the program Geneious (www.geneious.com) was used for Bayesian analyses with the following settings: 1 million replicates, WAG substitution model, 4 heated chains, 25% burnin, and subsample frequency of 1000. Consensus tree images were saved through Geneious and then manipulated in Adobe Photoshop. Only bootstrap values over 50 are shown. Species used: Adi=*Acropora digitifera*; Ag=*Anopheles gambiae*; Bf=*Branchiostoma floridae*; Bt=*Bos taurus*; Ct=*Capitella teleta*; Dm=*Drosophila melanogaster*; Dr=*Danio rerio*; Gg=*Gallus gallus*; Hs=*Homo sapiens*; Nvit=*Nematostella vectensis*; Sp=*Strongylocentrotus purpuratus*; Sm=*Schmidtea mediterranea*; Xl=*Xenopus laevis*; Xt=*Xenopus tropicalis*. *S. mediterranea* homologs are in red fonts.

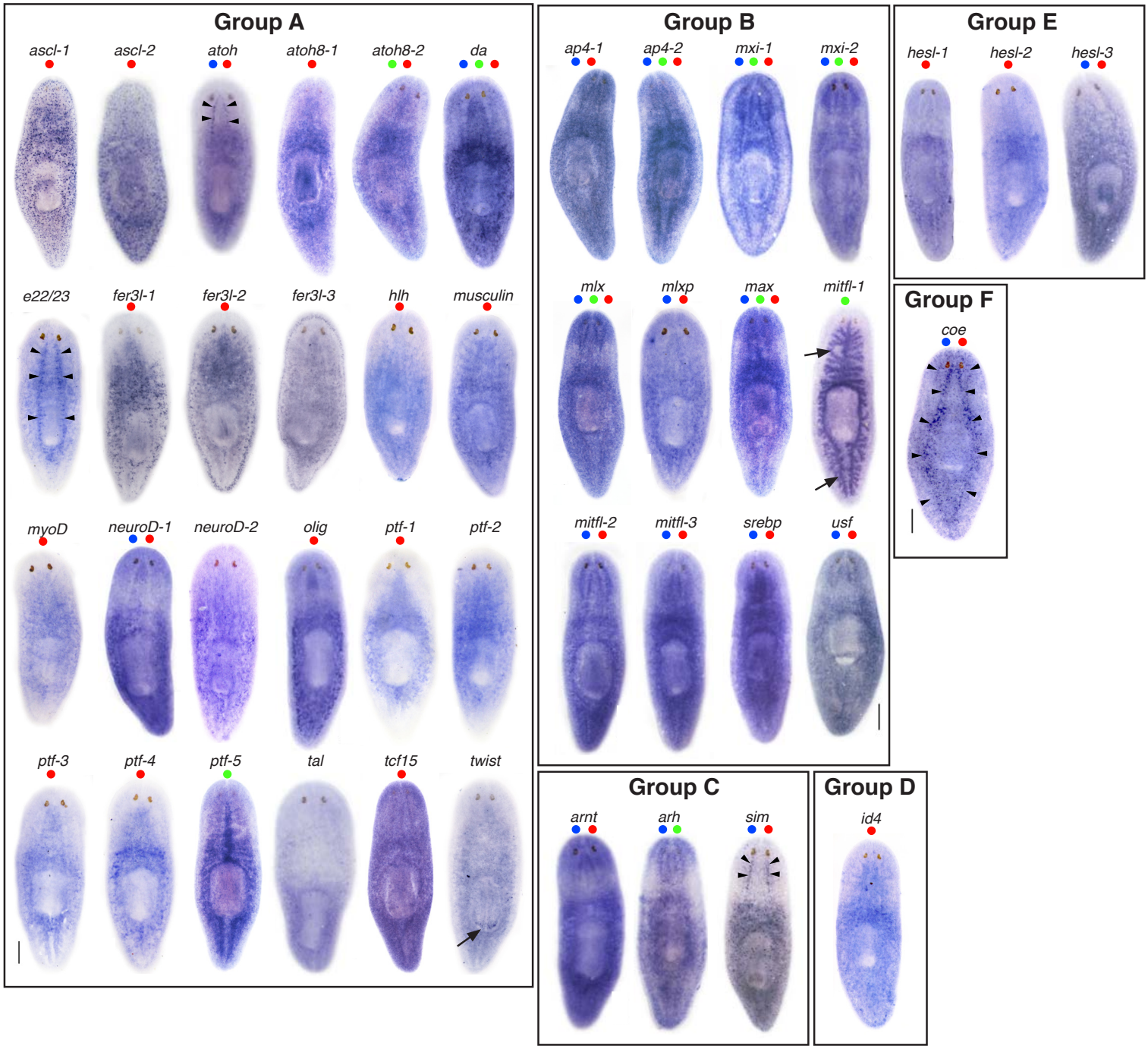

Fig. S2: Expression analysis of bHLH genes in *S. mediterranea*. Intact animals were processed for whole-mount in situ hybridization to bHLH genes. Gene names are indicated above each animal. bHLHs were expressed in a wide range of cells and tissues. *ascl-1* and *ascl-2* were expressed in a punctate pattern throughout the mesenchyme. *atoh*, *e22/23*, *sim*, and *coe* were expressed in distinct cells in the CNS (black arrowheads). *mitfl-1* and *twist* were exclusively detected in the intestine and pharynx (black arrows). Many bHLH genes, including *arnt*, *da*, *ap4-1*, *max* and *srebp*, were detected ubiquitously throughout the animal. *fer3l-1*, *fer3l-2*, and *fer3l-3* exhibited related expression patterns with *fer3l-1* expression detected in the interior mesechyme (stem cell-like) and *fer3l-2* and *fer3l-3* detected more exteriorly (similar to a post-mitotic progeny pattern). No definitive expression pattern was observed for *neuroD-2*. The expression of genes in planarian stem cells and immediate progeny is characterized by parenchymal (mesenchymal) staining ranging from punctate expression in stem cell or progeny to diffuse expression throughout the animal and γ-irradiation sensitive. As expected, most bHLHs displayed reduced expression following γ-irradiation (see Table S1). Blue and green dots above the animals denote expression in the CNS and intestine, respectively; red dots denote genes that were γ-irradiation sensitive. Genes were categorized in bHLH Groups A-F based on their homology. Scale bars = 200 μm.

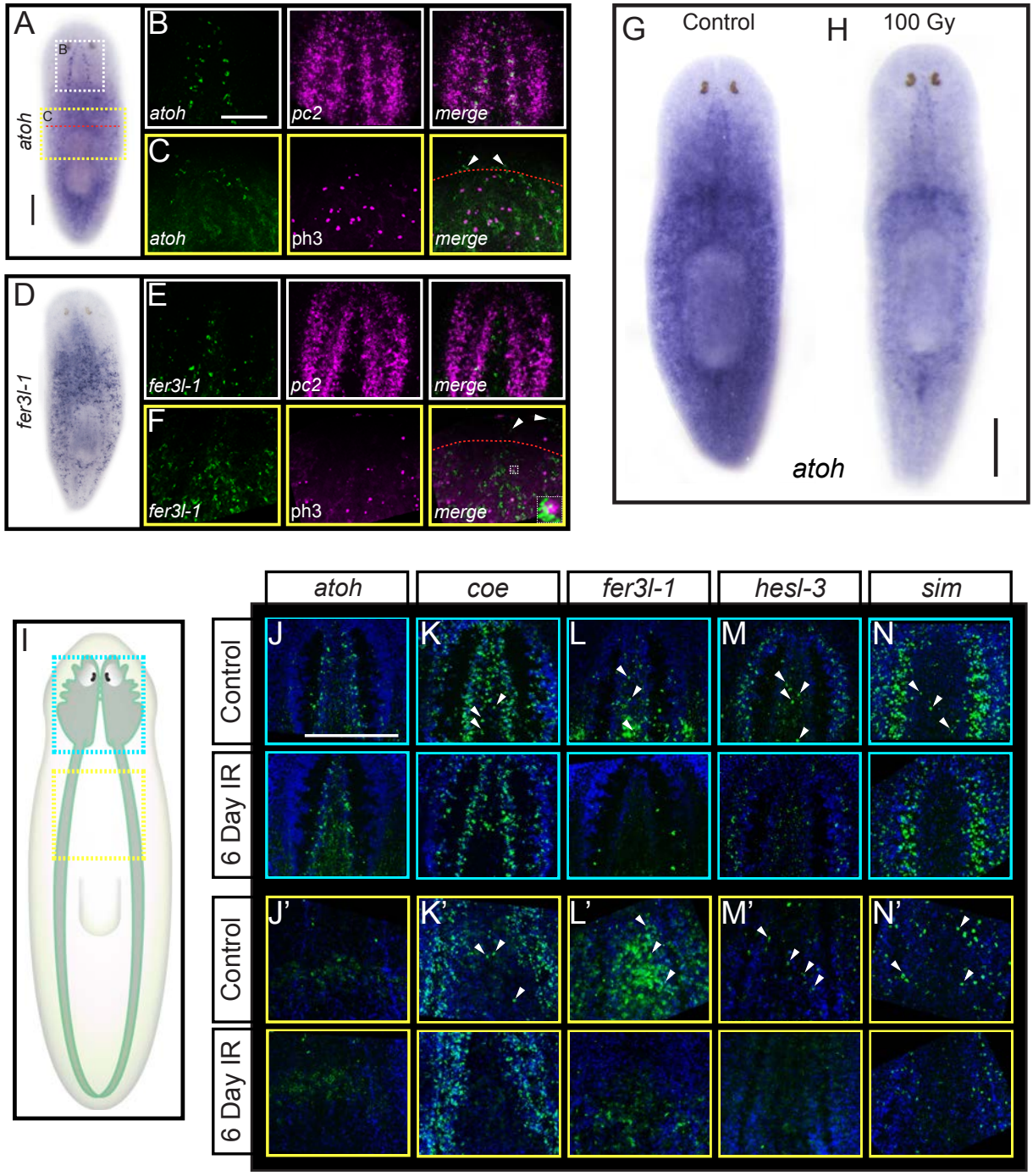

Fig. S3: bHLH genes are expressed in γ-irradiation-sensitive populations near the CNS and stem cell compartment. (A) Expression pattern of atoh. Dashed boxes indicate zoom area of the brain or regeneration blastema shown in B and C, respectively. Dashed red line indicates site of amputation. (B) FISH to *atoh* (green) and *pc2* (magenta). (C) FISH to *atoh* counterstained with anti-phosphohistone-H3 (ph3) to label mitotic cells in 3 day regenerates. Arrowheads denote *atoh*$^{+}$ cells within the blastema. (D-F) show similar analysis for *fer3l-1*. White dashed box in F highlights a bHLH/ph3-positive cells shown at high magnification within the merged image inset. (G and H) WISH to *atoh* in controls or animals 6 days post-irradiation (100 Gy). (I) Cartoon depicting the planarian CNS; blue (head) and yellow (pre-pharyngeal) boxes denote areas of the animal imaged in J-N and J'-N', respectively. (J-N') Control and γ-irradiated animals processed for fluorescent in situ hybridization to *atoh*, *coe*, *fer3l-1*, *hesl-3*, and *sim*, and counterstained with DAPI. Arrowheads denote representative cell populations lost following γ-irradiation. Scale bars = 200 μm.

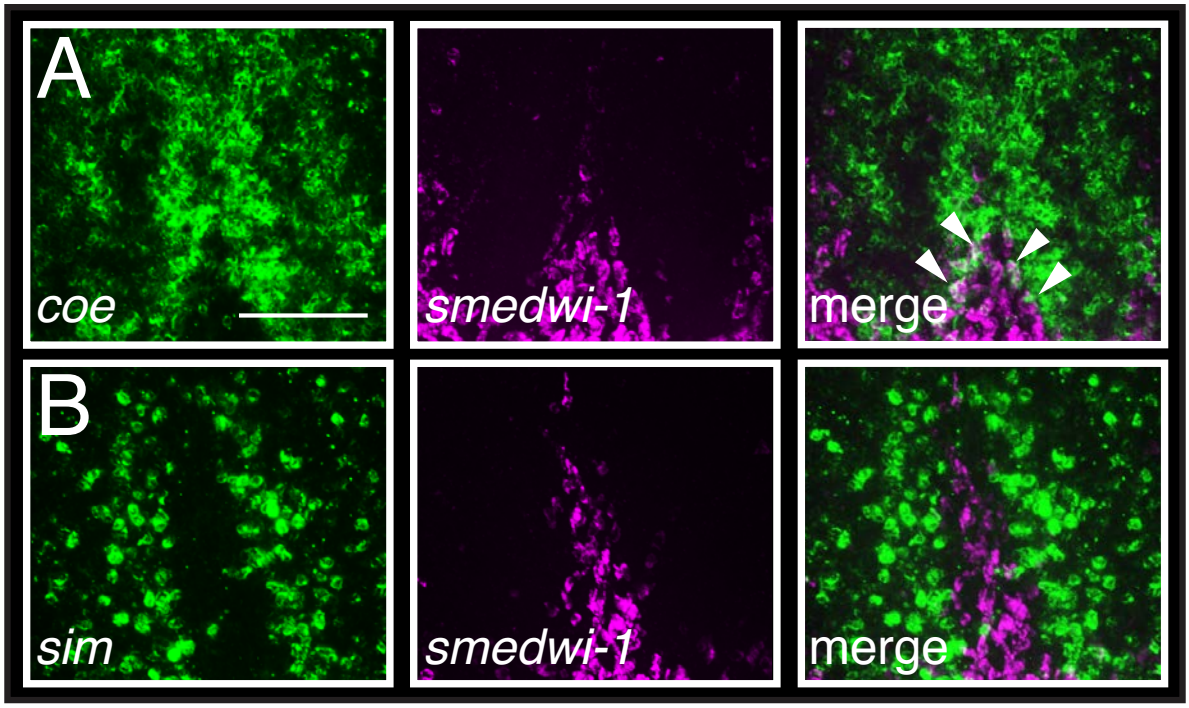

Fig. S4: *coe* and *sim* are not co-expressed with *smedwi-1* in the anterior region of the cephalic ganglia. (A-B) Representative images from the head region of animals processed for double-fluorescent in situ hybridization to *coe* or *sim* and *smedwi-1*. White arrows point to *coe*$^{+}$/*smedwi-1*$^{+}$ cells. Scale bar in A = 100 μm.

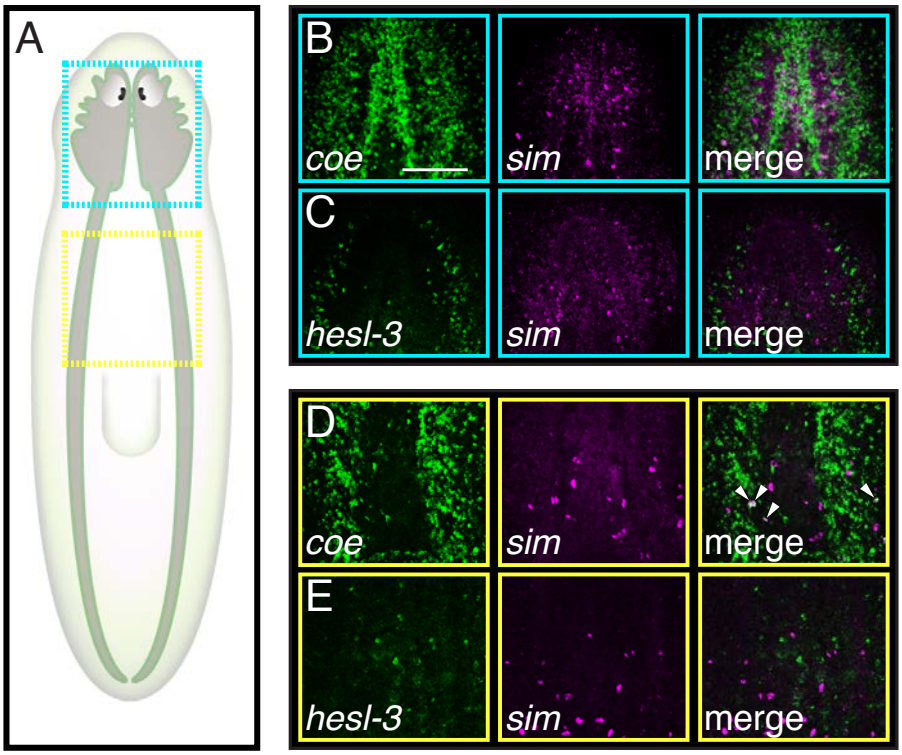

Fig. S5: *coe* and *sim* are co-expressed in cells in the pre-pharyngeal area. (A) Cartoon depicting the planarian CNS. Blue (head) and yellow (pre-pharyngeal) boxes denote the region of the animal imaged in B-D, respectively. (B-E) Images of the brain region of animals processed for double-fluorescent in situ hybridization to *coe* and *sim* or *hesl-3* and *sim*. Scale bar in B = 100 μm.

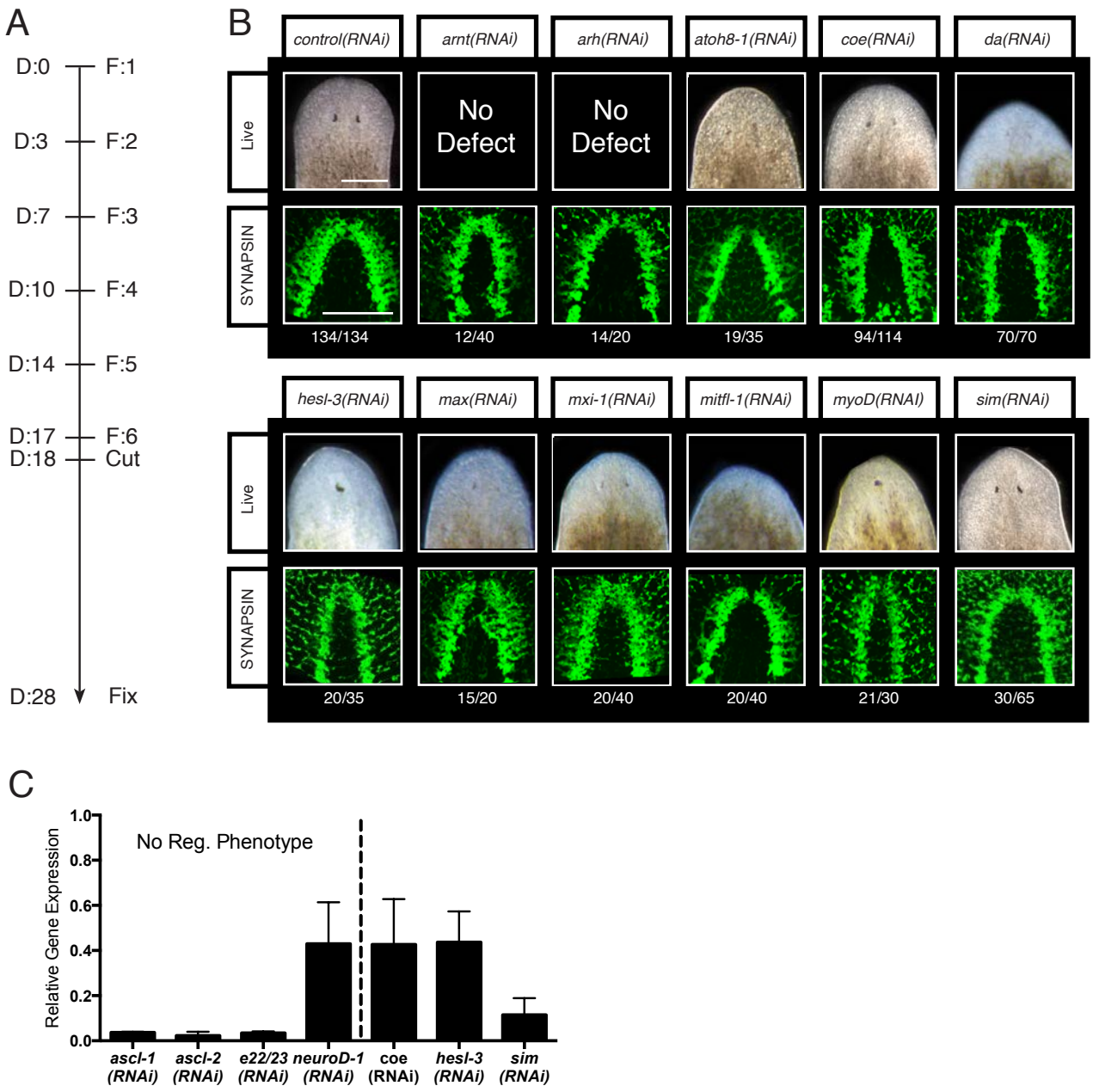

Fig. S6: bHLH RNAi screen for defects in CNS regeneration. (A) Experimental design for RNAi screen; D and F denote days and number of bacterial feedings, respectively. (B) Summary of RNAi phenotypes following bHLH knockdowns. Images shown are of 10-day regenerates. Numbers below images refer to the number of animals with an observable regeneration defect. (C) Quantitative real-time PCR measurements of relative mRNA expression after RNAi knockdown of selected bHLH genes. *ascl-1*, *ascl-2*, *e22/23* and *neuroD-1* did not result in a regeneration phenotype following RNAi. Scale bars = 200 μm

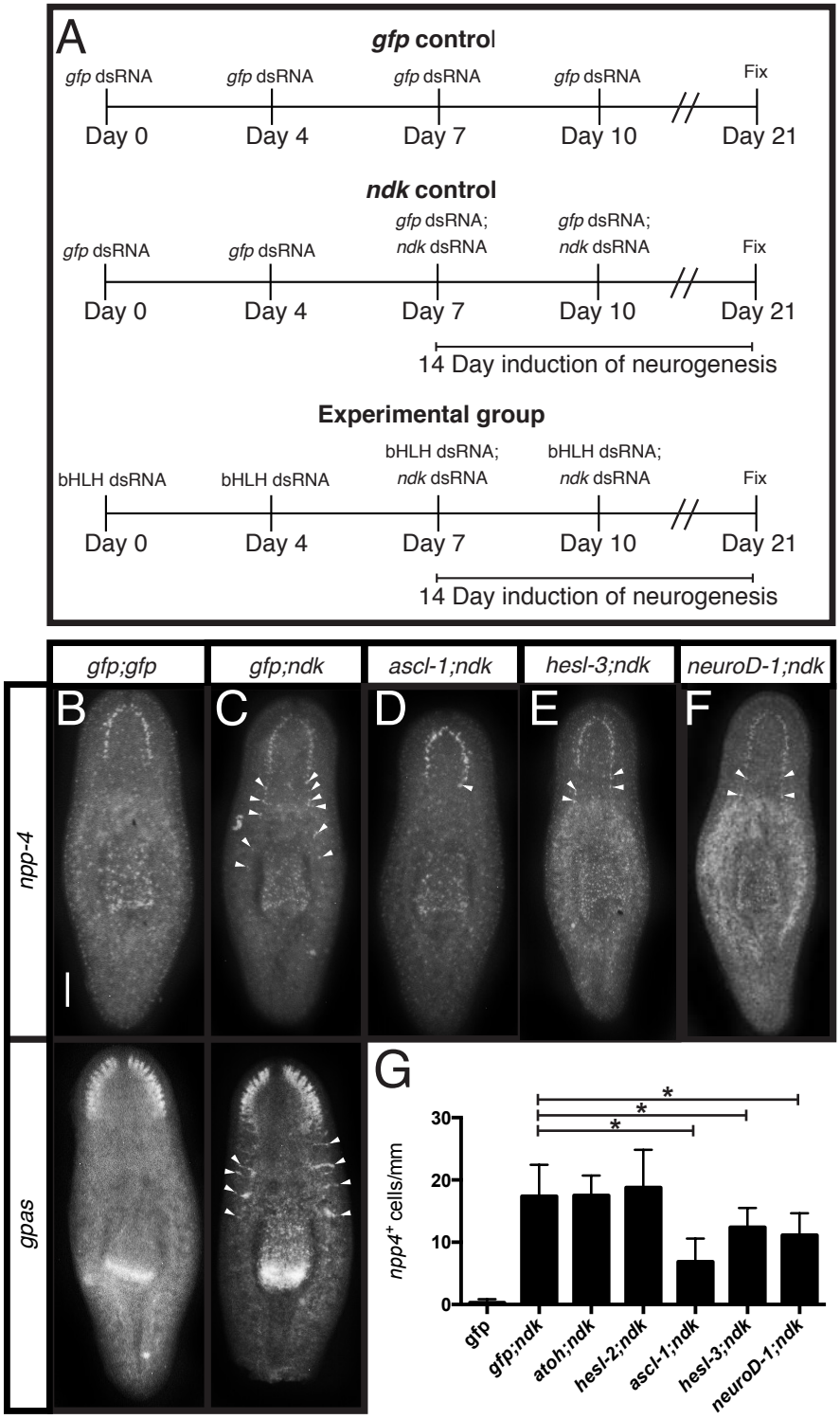

Fig. S7. *ascl-1*, *hesl-3,* and *neuroD-1* suppress ectopic formation of *npp-4*⁺ cells when co-silenced with *ndk*. (A) Schematic of RNAi-based suppression assay. For double knockdown experiments, bacterial pellets containing dsRNA for each gene were mixed 1:1. For select bHLH and ndk co-silencing experiments, planarians were fed dsRNA four times over two weeks. The first two RNAi feedings contained *bHLH* dsRNA and the final two RNAi treatments contained both *bHLH* and *ndk* dsRNA. (B-F) *gfp;gfp(RNAi)*, *gfp;ndk(RNAi)*, *ascl-1;ndk(RNAi), hesl-3;ndk(RNAi)*, and *neuroD-1;ndk(RNAi)* animals were processed for FISH to *npp-4* or *gpas*. (G) Quantification of ectopic *npp-4*⁺ cells (arrowheads in B-F of top row; n > 9 animals per group); neurons were normalized by the length of the animal (mm). Asterisks denote a significant reduction of cells when compared with *gfp;ndk(RNAi)* animals ($p < 0.05$, Student's t-test). The expansion of *gpas* after *ndk* RNAi (arrowheads in B and C of bottom row) was not affected after *bHLH* knockdowns. Scale bar = 200 μm.

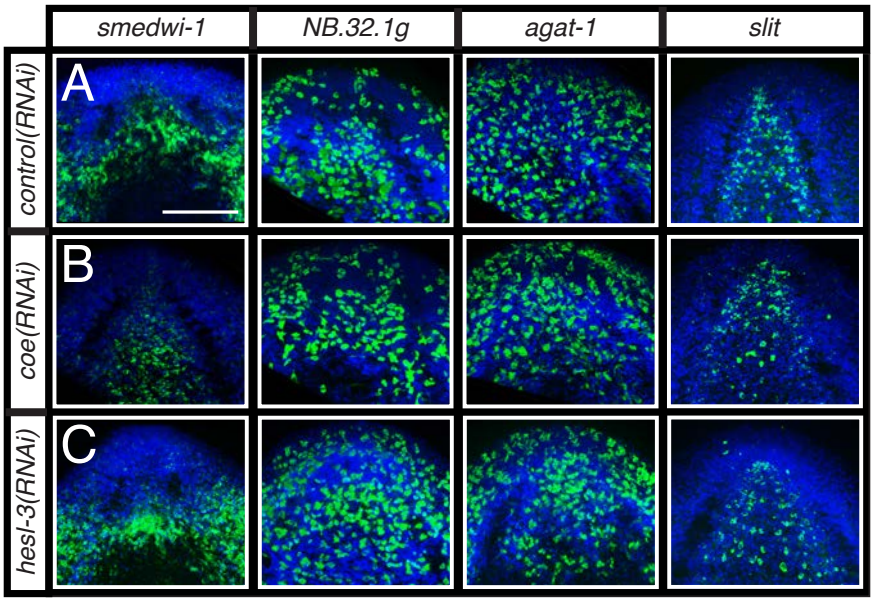

Fig. S8: *coe* and *hesl-3* RNAi phenotypes are not due to a loss of the stem cells, progeny, or midline signals. (A-C) RNAi treated animals were amputated, allowed to regenerate for 5 days, and then processed for fluorescent in situ hybridization to *smedwi-1*, *NB.32.1g*, *agat-1*, or *slit* and counterstained with DAPI. Scale bar = 100 μm.

Movie 1. *control(RNAi)* intact planarians display the stereotypical light avoidance response and glide away from the center of the petri dish.

Movie 2. *coe(RNAi)* intact animals fail to display a robust response to light. Some animals do not show normal locomotion behaviors and appear to be immobilized.

Movie 1

Movie 2

Table S1. Summary of bHLH homologs in S. mediterranea and their expression patterns determined from published RNA-seq data and in situ hybridization.

Gene Name	Top Hit Accession	Top Hit Gene Name	Top Hit Evalue	Category	cRPKM SC *	cRPKM Prog *	cRPKM Diff *	log2(X1/Xins) #	log2(X1/X2) #	log2(X2/Xins) #	Category	Stem Cells/Progeny	CNS	Pharynx	Intestine	Epidermis	Mesenchyme
Smed-achaete scute like-1 (ascl-1)	Q6XD76	ASCL4_HUMAN	4.00E-11	*A*	19.03	34.14	40.22	-2.811263821	-0.481553859	-2.329709962	6	Yes	No	No	No	No	Yes
Smed-achaete scute like-2 (ascl-2)	Q9NQ33	ASCL3_HUMAN	7.00E-19	*A*	1.17	2.77	3.71	0.763645015	0.596177444	0.167467571	2	Yes	No	No	No	No	Yes
Smed-activating enhancer binding protein-like-4-1 (ap4-1)	Q01664	TFAP4_HUMAN	1.00E-15	*B*	4.22	7.75	7.75	-1.723158391	-0.159717879	-1.563440512	6	Yes	Yes	Yes	No	No	Yes
Smed-activating enhancer binding protein-like-4-2 (ap4-2)	Q01664	TFAP4_HUMAN	4.00E-15	*B*	153.27	150.92	17.96	1.814102441	0.554289807	1.259812634	1	Yes	Yes	Yes	Yes	No	Yes
Smed-aryl hydrocarbon receptor (ahr)	Q95LD9	AHR_DELLE	1.00E-95	*C*	0.75	10.49	7.26	-1.699145616	-1.970169379	0.271023763	3	No	Yes	No	No	Yes	Yes
Smed-aryl hydrocarbon receptor nuclear translocator-like (arnt)	O15945	ARNT_DROME	2.00E-149	*C*	31.88	58.94	10.93	2.222109911	0.722122834	1.499987077	1	Yes	Yes	No	No	No	Yes
Smed-atonal homolog (atoh)	P48985	ATOH1_MOUSE	3.00E-15	*A*	NA	NA	NA	2.026679421	-2.047678746	4.074358167	3	Yes	Yes	No	No	No	Yes
Smed-atonal homolog 8-1 (atoh8-1)	Q99NA2	ATOH8_MOUSE	8.00E-21	*A*	9.74	9.03	6.23	1.723287277	0.225953792	1.497333485	1	Yes	No	Yes	No	No	Yes
Smed-atonal homolog 8-1 (atoh8-2)	Q99NA2	ATOH8_MOUSE	2.00E-21	*A*	8.19	16.3	5.1	0.289713827	-0.110414501	0.400128328	3	Yes	No	Yes	Yes	No	Yes
Smed-basic helix-loop-helix family, member e22/23-like (e22/23)	Q8BGW3	BHE23_MOUSE	1.00E-34	*A*	0.93	2.17	17.47	-4.017714699	-4.003735398	-0.0139793	5	No	Yes	No	No	No	Yes
Smed-collier (coe)	Q63398	COE1_RAT	0	*F*	7.27	27.86	11.33	1.493145159	-0.638989339	2.132134498	3	Yes	Yes	Yes	No	No	Yes
Smed-daughterless (da)	P11420	DA_DROME	3.00E-41	*A*	53.33	49.7	19.05	2.52093294	1.485722114	1.035210826	1	Yes	Yes	Yes	Yes	Yes	Yes
Smed-fer3l-1 (fer3l-1)	Q9VGJ5	FER3_DROME	4.00E-31	*A*	31.02	16.89	8.73	1.063803447	2.014550656	-0.950747209	4	Yes	Yes	No	No	No	No
Smed-fer3l-2 (fer3l-2)	Q923Z4	FER3L_MOUSE	3.00E-26	*A*	5.67	16.56	7.59	-0.574771203	0.096606434	-0.671377637	6	Yes	No	No	No	No	Yes
Smed-fer3l-3 (fer3l-3)	Q9VGJ5	FER3_DROME	1.00E-23	*A*	0.08	0.6	11.46	-5.399585334	-1.725750651	-3.673834683	5	No	No	No	No	No	Yes
Smed-hairy and enhancer of split like-1 (hesl-1)	Q00P32	HES2_XENLA	2.00E-07	*E*	3.81	0	0.09	NA	NA	NA	NA	Yes	Yes	No	No	No	Yes
Smed-hairy and enhancer of split like-2 (hesl-2)	Q03062	HES5_RAT	4.00E-15	*E*	4.51	0.92	0.96	3.274606934	2.844104957	0.430501977	2	Yes	No	No	No	No	Yes
Smed-hairy and enhancer of split like-3 (hesl-3)	Q7KM13	HEY_DROME	3.00E-30	*E*	11.96	0.78	0.18	4.684890904	3.447034004	1.237856899	2	Yes	Yes	No	No	No	Yes
Smed-helix-loop-helix 1 (hlh1)	Q02576	HEN1_MOUSE	4.00E-25	*A*	NA	NA	NA	NA	NA	NA	NA	Yes	Yes	No	No	No	Yes
Smed-inhibitor of DNA binding 4 (id4)	P47928	ID4_HUMAN	7.00E-13	*D*	7.7	8.45	17.52	0.102628274	-1.151843339	1.254471613	3	Yes	Yes	No	No	No	Yes
Smed-max-interactor-1 (mxi-1)	P50538	MAD1_MOUSE	6.00E-07	*B*	14.78	31.8	35.8	-0.057960799	-0.965995962	0.908035162	3	Yes	Yes	Yes	Yes	No	Yes
Smed-max-interactor-2 (mxi-2)	P50541	MXI1_DANRE	2.00E-06	*B*	5.62	13.45	48.55	-1.57110712	-0.895675653	-0.675431468	5	Yes	Yes	Yes	Yes	No	Yes
Smed-max-like protein x (mlx)	Q9UH92	MLX_HUMAN	4.00E-33	*B*	100.4	142.72	48.91	1.290308875	0.461109763	0.829199113	1	Yes	Yes	Yes	Yes	No	Yes
Smed-microphthalmia-associated transcription factor like-1 (mitfl-1)	Q08874	MITF_MOUSE	5.00E-12	*B*	1.21	2.12	17.32	-3.793499542	-1.403822556	-2.389676985	5	No	No	No	No	No	No
Smed-microphthalmia-associated transcription factor like-2 (mitfl-2)	Q6XBT4	USF1_BOVIN	1.00E-09	*B*	19.43	37.69	19.44	0.77606873	0.36519556	0.41087317	1	Yes	Yes	No	No	No	Yes
Smed-microphthalmia-associated transcription factor like-3 (mitfl-3)	P19484	TFEB_HUMAN	7.00E-08	*B*	21.67	8.28	10.94	1.528466439	1.822857224	-0.294390785	2	Yes	Yes	No	No	No	Yes
Smed-mlx interacting protein-like (mlxipl)	Q99MZ3	MLXPL_MOUSE	5.00E-27	*B*	9.43	19.65	15.04	-0.15075684	-0.033276976	-0.117479864	6	Yes	Yes	No	No	No	Yes
Smed-musculin	A8E5T6	TCF21_XENTR	1.00E-20	*A*	5.1	0.63	0.59	NA	NA	NA	NA	Yes	Yes	No	No	No	Yes
Smed-MYC assciated factor X (max)	P52164	MAX_RAT	2.00E-16	*B*	71.58	160.14	56.55	1.136004411	-0.171197368	1.30720178	1	Yes	Yes	Yes	Yes	Yes	Yes
Smed-myogenic differentiation (myoD)	Q91154	MYF5_NOTVI	2.00E-39	*A*	12.6	11.04	14.73	1.187144093	1.071515453	0.11562864	2	Yes	No	No	No	No	Yes
Smed-neurogenic differentiation-1 (neuroD-1)	Q6NYU3	NDF6A_DANRE	9.00E-41	*A*	12.21	2.97	0.83	3.693436013	2.125430512	1.568005501	1	Yes	Yes	No	No	No	Yes
Smed-neurogenic differentiation-2 (neuroD-2)	Q9HD90	NDF4_HUMAN	4.00E-11	*A*	2.64	1.22	2.03	-0.422627981	-1.837809158	1.415181178	3	NA	NA	NA	NA	NA	NA
Smed-oligodendrocyte lineage transcription factor (olig)	Q90XB3	OLIG2_CHICK	2.00E-30	*A*	8.2	0.38	0.22	NA	NA	NA	NA	Yes	No	No	No	No	Yes
Smed-pancreas specific transcription factor-1 (ptf-1)	Q7RTS3	PTF1A_HUMAN	7.00E-26	*A*	2.5	0.22	2.2	NA	NA	NA	NA	Yes	No	No	No	No	Yes
Smed-pancreas specific transcription factor-2 (ptf-2)	Q4ZHW1	PTF1A_XENLA	9.00E-33	*A*	0.21	0.39	2	NA	NA	NA	NA	No	No	No	No	No	Yes
Smed-pancreas specific transcription factor-3 (ptf-3)	Q20561	HLH13_CAEEL	8.00E-24	*A*	0.26	0	2.46	NA	NA	NA	NA	Yes	No	No	No	No	Yes
Smed-pancreas specific transcription factor-4 (ptf-4)	Q4ZHW1	PTF1A_XENLA	3.00E-33	*A*	0.82	6.1	20.36	-2.246339074	-3.884949246	1.638610172	3	Yes	No	No	No	No	Yes
Smed-pancreas specific transcription factor-5 (ptf-5)	Q8AW52	ATOH7_DANRE	2.00E-12	*A*	0.18	3.23	11.07	-1.764733957	-2.389883365	0.625149408	3	No	No	Yes	Yes	No	Yes
Smed-single minded (sim)	A2T6X9	SIM1_PANTR	6.00E-161	*C*	14.74	6.15	2.52	4.884660416	2.869195938	2.015464478	1	Yes	Yes	Yes	No	No	Yes
Smed-sterol regulatory element binding transcription factor (srebp)	A3KNA7	SRBP2_DANRE	3.00E-15	*B*	17.13	46.46	28.97	0.46831113	-0.298806385	0.767117515	3	Yes	Yes	Yes	No	No	Yes
Smed-T-cell acute lymphocytic leukemia (tal)	P17542	TAL1_HUMAN	9.00E-17	*A*	0.23	3.69	6.45	-4.330872584	-5.062034039	0.731161455	3	No	No	No	No	No	Yes
Smed-transcription factor 15 (tcf15)	P79782	TCF15_CHICK	3.00E-23	*A*	59.67	20.65	14.63	1.723522574	0.927041018	0.796481556	1	Yes	No	Yes	No	No	Yes
Smed-twist	Q9D030	TWST2_MOUSE	1.00E-32	*A*	2.31	1.74	0.25	4.980875731	1.462910913	3.517964818	1	No	No	Yes	No	No	Yes
Smed-upstream transcription factor (usf)	Q15853	USF2_HUMAN	1.00E-09	*B*	32.3	32.87	30.57	1.168698426	0.706880908	0.461817517	1	Yes	Yes	No	No	No	Yes

A = 24
B = 12
C = 3
D = 1
E = 3
F = 1

* Labbe et al. 2012

\# Onal et al. 2012

35/43 in Stem Cells
25/43 in CNS
33/43 in Stem Cells or CNS
23/43 in Stem Cells and CNS
NA: Unable to detect by WISH

Table S2. Accession numbers and oligonucleotide sequences to clones used in this study.

bHLH Clones

Gene Name	Accession Number	Forward Primer	Reverse Primer
Smed-achaete scute like-1 (ascl-1)	DN307058	NA	NA
Smed-achaete scute like-2 (ascl-2)	KF487091	CCGCTCGAGTGGGTTGCTTATCCAGAAATG	ATAAGAATGCGGCCGCGACTCGTCGATATCTTGTTCTTT
Smed-activating enhancer binding protein-like-4-1 (ap4-1)	DN305431	NA	NA
Smed-activating enhancer binding protein-like-4-2 (ap4-2)	HO007476	NA	NA
Smed-aryl hydrocarbon receptor (ahr)	KF487107	CATTACCATCCCGCCCGACACAGGAATCAACTG	
Smed-aryl hydrocarbon receptor nuclear translocator (arnt)	KF487108	CATTACCATCCCGCCGATAGAGACCAAGAGCAAATAG	
Smed-atonal homolog (atoh)	Sequence Below	CCGCTCGAGAAACAACCAGCCGACTCAAC	ATAAGAATGCGGCCGCCGTTTGAGCCATTAATAGAGTTTC
Smed-atonal homolog 8-1 (atoh8-1)	DN306140	NA	NA
Smed-atonal homolog 8-2 (atoh8-2)	HO006843	NA	NA
Smed-basic helix-loop-helix family, member e22/23-like (e22/23)	KF487092	CCGCTCGAGAGACTGTTGCGGCTCGAC	ATAAGAATGCGGCCGCTGCGACATAAAATACAAATTGC
Smed-collier (coe)	KF487109	CATTACCATCCCGCGTTTTGAACCATGCTTCG	
Smed-daughterless (da)	KF487093	CCGCTCGAGCGAAGAGCAGACAACAGCAC	ATAAGAATGCGGCCGCTTTTACCAACACCCGATTGC
Smed-fer3l-1 (fer3l-1)	KF487094	CCGCTCGAGTTAAGTCAAATCAGGAACCTC	ATAAGAATGCGGCCGCTGCCGTTCAAAAGTTCAGTC
Smed-fer3l-2 (fer3l-2)	KF487095	CCGCTCGAGATTCGACTGAAATGACTGAAATC	ATAAGAATGCGGCCGCCAACCGCAATGTTTCAATTC
Smed-fer3l-3 (fer3l-3)	KF487096	CCGCTCGAGAGAAACCCCAGCCATTTTTC	ATAAGAATGCGGCCGCAATTTGTCGATCATTTTTCAGG
Smed-hairy and enhancer of split like-1 (hesl-1)	KF487110	CATTACCATCCCGGAAATGGAAAGACGACGAAGGGCG	
Smed-hairy and enhancer of split like-2 (hesl-2)	KF487111	CATTACCATCCCGTCGCCGACAGAGAATAAATTTCGC	
Smed-hairy and enhancer of split like-3 (hesl-3)	KF487112	CATTACCATCCCGCTTGAGCCAGATCAATATCACAGC	
Smed-helix-loop-helix 1 (hlh1)	KF487113	CATTACCATCCCGGATGAATCGTGGTCGAAATTGAGC	
Smed-inhibitor of DNA binding 4 (id4)	KF487114	CATTACCATCCCGAAACTCGTTCCAACGATTCC	
Smed-max-interactor-1 (mxi-1)	KF487115	CATTACCATCCCGAGATTCCGTACCCTGTCGAATTAC	
Smed-max-interactor-2 (mxi-2)	KF487116	CATTACCATCCCGACCCTGGAAGGATCAGAATTGGAC	
Smed-max-like protein x (mlx)	HO006087	NA	NA
Smed-microphthalmia-associated transcription factor like-1 (mitfl-1)	KF487117	CATTACCATCCCGCGCACTCGAAAGCAATTATC	
Smed-microphthalmia-associated transcription factor like-2 (mitfl-2)	KF487118	CATTACCATCCCGTGAAGTCTCGCACAAATGCTCAAC	
Smed-microphthalmia-associated transcription factor like-3 (mitfl-3)	KF487119	CATTACCATCCCGTAAAACGACGACGATCACACAGTC	
Smed-mlx interacting protein-like (mlxipl)	KF487097	CCGCTCGAGAGTTTCGGGACAGTCGTTC	ATAAGAATGCGGCCGCACGGGTTTATTTGTTGCTG
Smed-musculin	KF487098	CCGCTCGAGAAACGTCGTGGTCGTAAACC	ATAAGAATGCGGCCGCCCTCCAGGAACTAATTGACATCG
Smed-MYC asscciated factor X (max)	DN308448	NA	NA
Smed-myogenic differentiation (myoD)	KF487099	CCGCTCGAGTTTCCAGGTTCCACTTGTCC	ATAAGAATGCGGCCGCTCCTAGTCGTCGGGAGTTTG
Smed-neurogenic differentiation-1 (neuroD-1)	DN305764	NA	NA
Smed-neurogenic differentiation-2 (neuroD-2)	KF487120	CATTACCATCCCGGATTTAGGGAAACTCATTGC	
Smed-oligodendrocyte lineage transcription factor 2 (olig2)	KF487100	CCGCTCGAGACCTGAATTCGGCATTGGAC	ATAAGAATGCGGCCGCCCAATAGGAAACTCTTTCAAG
Smed-pancreas specific transcription factor-1 (ptf-1)	KF487101	CCGCTCGAGAGCCGCAAACATGAGAGAAC	ATAAGAATGCGGCCGCGCCAAAGAATAAGGCAGATGG
Smed-pancreas specific transcription factor-2 (ptf-2)	KF487102	CCGCTCGAGCTGATGGAGCCTTTCGGATT	ATAAGAATGCGGCCGCTCATTCCTTTCAACAACACGA
Smed-pancreas specific transcription factor-3 (ptf-3)	KF487103	CCGCTCGAGCGTTTACTTATCAAAATCCTTCTACG	ATAAGAATGCGGCCGCAATGCTGTCGTTGGGTTCAC
Smed-pancreas specific transcription factor-4 (ptf-4)	KF487104	CCGCTCGAGCACTTGCGATTCGTCATAACAG	ATAAGAATGCGGCCGCTCGGTTCCCTGATATTCCTC
Smed-pancreas specific transcription factor-5 (ptf-5)	DN303577	NA	NA
Smed-single minded (sim)	KF487121	CATTACCATCCCGGCGTCTATTATTCGACTGACATCG	
Smed-sterol regulatory element binding transcription factor (srebp)	KF487122	CATTACCATCCCGAAATTCCCCACCCAATGAAC	
Smed-T-cell acute lymphocytic leukemia (tal)	KF487105	CCGCTCGAGTTGTAGGAAACCAATCTCAACG	ATAAGAATGCGGCCGCTTCAAGATTTCTTCCAGAATCC
Smed-transcription factor 15 (tcf15)	AFD29618	NA	NA
Smed-twist	KF487106	CCGCTCGAGCAAGAAAGAACAGAATCATATTTGG	ATAAGAATGCGGCCGCCCCAAGCTCCTTCCATTCTC
Smed-upstream transcription factor (usf)	KF487123	CATTACCATCCCGTGTTTCGATTTGTTCCCGTG	

Other Clones

Gene Name	Accession Number
Smed-agat-1	DN290976
Smed-ChAT	FG310880
Smed-cpp-1	BK007012
Smed-gpas	HQ121519
Smed-h2b	DN298006
Smed-npp-4	BK007037
Smed-npy-2	BK007019
Smedwi-1	DN309285
NB.32.1g	DN298711
Smed-pc2	BK007043

qPCR Primers

Target	Forward Primer	Reverse Primer
Smed-β-tubulin	TGGCTGCTTGTGATCCAAGA	AAATTGCCGCAACAGTCAAATA
Smed-ascl-1	TCTCAATACCCCTTCAATCATG	TGCAGTCGTAACCCGATTTC
Smed-ascl-2	TTTCAATTACCCAGTTCCCTTTC	CGTTCTCTTTCATTGCGTCTC
Smed-coe	CTGCAACGCTGGATCAACTA	TGGCTGATTGCTTCTTCCTT
Smed-e22/23	CGTATGCTCACAGTCCATCG	ATATCCTCGGGACTGGAACC
Smed-hesl-3	CAAAACCAGCCGATTCATTATC	TCGCAATGTTTGTCGGATAC
Smed-neuroD-1	CTCTAATCAAACCGGGCAAG	ATGGAAATGGACCTTGGATG
Smed-sim	AGTCGAATTAACCGGCAATAG	GCTTGGTACTGGTGATGGTAAG

>Smed-atonal homolog (atoh)

AAACAACCAGCCGACTCAACTTACCAAATCGAATCCTATCAAACGGACCGCAGCCAACGACAGAGAACGAAAACGAATGTATTGTTTGAACCGAGCCTTTGACCAACTGAGAGATGTCGTTCCTTACTCTTCT
AATCAAAAGAAAATGTCAAAGTTTGAAACTCTATTAATGGCTCAAACG